Theoretical and Experimental Investigation of Binding of Small Molecular Weight Drugs to Proteins

by

Selimcan Azizoğlu

A Thesis Submitted to the

Graduate School of Engineering

in Partial Fulfillment of the Requirements for

the Degree of

Master of Science

in

Chemical and Biological Engineering

Koç University

September, 2011

Koç University

Graduate School of Sciences and Engineering

i

This is to certify that I have examined this copy of a master's thesis by

Selimcan Azizoğlu

and have found that it is complete and satisfactory in all respects,

and that any and all revisions required by the final

examining committee have been made.

Committee Members:

_____

Seda Kızılel Ph.D. (Advisor)

_____

Burak Erman Ph.D.

_____

Rıza Kızılel Ph.D.

Date: _____

To Baran Azizoğlu

ABSTRACT

In this study, interaction of small molecular weight drug compounds with proteins has been characterized. The binding constants of interactions were first theoretically calculated using molecular docking simulations. Next, these interactions were experimentally investigated via Surface Plasmon Resonance (SPR). The theoretical binding constants, K_D, predicted from theoretical calculations have been compared with the experimental values obtained from SPR. As a model protein, *Escherichia coli (E.coli)* DNA photolyase was used due to its known crystal structure. Among the eight drugs analyzed, theoretical and experimental values have shown similar binding affinities between selected drug and protein pairs. The results obtained in this study may be significant to characterize the unknown interactions of existing drugs with various proteins.

ÖZET

Bu çalışmada, küçük molekül ağırlıklı ilaçların proteinler ile etkileşimleri incelenmiştir. İlk olarak, bu etkileşimin bağlanma sabitleri teorik olarak simülasyon programıyla hesaplanmıştır. Sonrasında, ilgili bağlanma sabitleri Yüzey Plazmon Rezonansı (YPR) tekniği yardımıyla deneysel olarak belirlenmiştir. Hesaplanan teorik bağlanma sabitleri, K_D, ile YPR'den alınan deneysel veriler karşılaştırılmıştır. Bu tez çalışmasında, kristal yapısı bilinen *Escherichia coli* (*E. coli)* DNA photolyase enzimi, model protein olarak kullanılmıştır. İlgili protein ve sekiz ilacın etkileşimleri, hem teorik olarak hem de deneysel olarak incelenmelerinin sonunda, iki teknikle de elde edilen verilerin benzer olduğu görülmüştür. Bu çalışmada uygulanan tekniklerin, ilaçların henüz bilinmeyen yan etkilerinin ortaya çıkartılmasında önemli olabileceği gösterilmiştir.

Acknowledgements

It is a pleasure to thank the many people who made this thesis possible.

First I offer my sincerest gratitude to my supervisor, Asst. Prof. Seda Kızılel who has supported me throughout my thesis with her patience and knowledge. I would also like to thank Prof. Burak Erman for his superior guidance and innovative approaches; I was one of the luckiest students to have the chance of being his student. Special and foremost thanks go to Dr. Rıza Kızılel for his guidance. One simply could not wish for a better and friendlier guidance. This page is not enough to express my gratitude for him.

I am thankful to Assoc. Prof. Halil Kavaklı for his assistance in this thesis. I would like to thank Hande Asimgil, Bilal Çakır, and Maja Marusic for protein expression and purification part of this thesis.

I would like to warmly thank Assoc. Prof. Fatoş Gökçen and Prof. Can Erkey for their refreshing, friendly discussions and advices.

Special thanks to Mümin Öztürk, Evrim Besray Ünal, Ece Bulut and Cemre Kocahakimoğlu for their endless help in computational part of this thesis. I would like to thank Enis Demir for SPR assays and to Caner Nazlı for scientific suggestions throughout this study.

End of 7 years at Koç University, I have to thank my friends working in the campus. Yalçın Abi and all Yemekçi crew, Erdoğan Abi and all ISS crew, Menaf Abi and all post office crew and all others not mentioned here. Of course, High 5 goes to Düşünebilen Çocuklar!

I wish to thank my entire extended family for providing a loving environment for me and to my most precious tear, Burcu.

Table of Contents

List of Tables

List of Figures

Chapter 1

General Introduction

1.1 Drug Discovery

Drug discovery is a multidisciplinary process which combines various areas (pharmacology, biology, chemistry, computational science, etc.) Emerging new technologies in chemistry, biotechnology as well as computational science & engineering has considerably changed drug discovery processes in the last few decades. Advances in molecular biology and biotechnology extensively helped scientists to have deeper insight into biochemical relations between drug and drug target (protein, enzyme, receptors, etc.) as well as specific production and mutation of both drugs and drug targets [1]. With the knowledge of three dimensional structure of biological target obtained through methods such as X-Ray crystallography or Nuclear Magnetic Resonance (NMR) spectroscopy, computer based molecular modeling techniques enabled virtual visualization and simulation of protein/drug interactions. Using structure based drug discovery approach; the binding of drug on a target protein is modeled and classified in terms of high affinity and selectivity of protein/drug interaction. Another major type of drug discovery is ligand-based drug discovery which is focused on the knowledge of other molecules binding to the biological target of interest [2].

Economic perspective of drug discovery is another issue yet to be explained. Figure 1.1 displays traditional drug discovery processes structured in eight steps [3]. The potent, safe drug candidate finally creates a return as market value. Each year around $50 billion is invested in drug discovery process by pharmaceutical companies worldwide. The entire final cost for one drug is estimated as approximately $800 million. If successfully marketed, the drug may return yearly turnover of $1 billion [4].

Target Discovery

Target Validation

Assay Development

Screening & Lead Discovery

Lead Optimization

Development

Clinical Trials

Marketing

Figure 1.1 Drug discovery process on a progression scale from early target discovery to clinical trials in human and marketing.

1.2 DNA photolyase/cryptochrome family proteins as drug target

Proteins from DNA photolyase/cryptochrome family function in various activities such as physiological repair of ultraviolet (UV) induced DNA damage, entrainment of circadian clock and stimulation of plant growth. Although proteins from this family have diverse functions, they have a common three-dimensional fold, sequence homology and redox-active flavin adenine dinucleotide (FAD) cofactor [5]

Photoreactivation is the process of repairing harmful effects of far UV (200 – 300 nm) on organisms by photoreactivating enzyme using blue light (350 - 450 nm) as an energy source. UV induced effects occur as the production of pyrimidine dimers in DNA. Two major DNA lesions are cyclobutane pryrimidine dimers (CPD) and pyrimidine-pyrimidine (6-4) photoproduct. A photolyase which repairs CPD cannot repair the other lesion, and vice versa. Thus, photolyases are referred in terms of which DNA lesion they repair. Another member of the family which has high sequence homology to photolyases but does not have photolyase activity is called cryptochrome. Cryptochrome plays a key role in regulation of blue light responses such as growth and development in plants, synchronization of circadian clock rhythm in animals [5]. The striking difference which results various functions among DNA photolyase/cryptochrome family member is the presence of C-terminal or N-terminal extensions in cryptochromes, which are

responsible in mediating the signal transduction step [1]. Table 1.1 gives the distribution of DNA photolyase/cryptochrome family member among different organisms.

Table 1.1 Photolyases and Cryptochromes in various organisms. V. cholera, *X. laevis*, *H. sapiens*, and *A. thaliana* contain two, three, two, and two cryptochrome genes, respectively. [5]

	DNA photolyase	(6-4)photolyase	cryptochrome
E. coli	+	-	-
B. subtilis	-	-	-
B. **firmus**	+	-	-
Synechocytis **sp.**	+	-	+
V. cholerae	+	-	+ (2)
M. thermoautotrophicum	+	-	-
M. Jannaschii	-	-	-
S. cerevisiae	+	-	-
S. pombe	-	-	-
C. elegans	-	-	-
D. melanogaster	+	+	+
X. laevis	+	+	+ (3)
H. sapiens	-	-	+ (2)
A. thaliana	+	+	+ (2)

DNA photolayse/cryptochrome proteins are flavoproteins which contain Flavin Adenin Dinucleotide and either methyltetrahydrofolate (MTHF) or 8-hydroxydeazaflavin (8-HDF) as the second cofactor. FAD is noncovalently bound to photolyase and active in two electron reduced form, (FADH$^-$). Although only FAD is essential cofactor for catalytic activity, the second cofactor significantly accelerates reaction rate since they have higher extinction coefficient than FADH$^-$ in the near UV/blue region, they absorb photoreactivation photons in sunlight in low-light conditions. By activation of light energy, electron transfer through excited flavin cofactor, FADH$^-$, breaks the pyrimidine dimer, resulting in photochemical repair [5].

1.3 Structure and Aim of the Thesis

Although there is strong research interest on DNA photolyase/cryptochrome family of proteins, structure and mechanism of these proteins are not very well known yet, especially in terms of inhibition and regulation of these proteins. With structure based characterization of drug-protein interaction, successful reversible inhibition of these proteins may result in

controlling functions of these enzymes such as DNA repair mechanism, circadian clock regulation.

In this thesis, the main objective is to determine high binding affinity and selectivity of an existing ligand/drug to the homologous active site of DNA photolyase/cryptochrome proteins (FAD region). This will be significant in order to make preliminary step for discovering a drug which can be used to inhibit/regulate the family proteins. *E. coli* DNA photolyase, whose three dimensional structures are very well known, the most studied enzyme among its family members, was selected to analyze photolyase/drug interaction.

This study includes combination of computational techniques with experimental measurements to characterize protein-drug binding. Chapter 2 examines computational approach which relies on virtual screening of molecular docking of drugs to the FAD region of *E. coli* DNA photolyase. Ligands for docking experiments were considered from U.S. Food and Drug Administration (FDA) approved drugs whose database is Super Drug Database with 2396 compounds (http://bioinformatics.charite.de/superdrug). FDA approved drugs were preferred since they are commercially available.

Chapter 3 is the beginning of experimental part of this thesis. First, *E. coli* DNA photolyase was expressed and purified to be used in real time experiments. Then, for further use in interaction analysis, photolyase was conjugated with Biotin-NHS. Detailed protocols for both expression and purification of *E. coli* DNA and its biotinylation steps are provided in Chapter 3.

Chapter 4 focuses Surface Plasmon Resonance (SPR) technology to perform real time analysis of photolyase/drug interaction. This chapter is the vital part of the thesis since computational studies in Chapter 3 are validated with experimental approach in terms of equilibrium dissociation constant, K_D.

Chapter 5 concludes the thesis with restating main findings and directing for further studies.

Chapter 2

Computational Approach

2.1 Introduction

Computational approaches using "molecular docking" helps scientist to predict the optimal energy and spatial configuration of one molecule to a second when bound to each other to form a stable complex [7]. In the last decade, molecular docking approach with virtual screening strategies has become an important part of drug discovery process.

In this thesis, the goal was to find a ligand/drug which has relatively high binding affinity and selectivity to the homologous active site of DNA photolyase/cryptochrome proteins (FAD region) in order to make preliminary step for discovering inhibitory or regulatory activity of a known drug towards family proteins. *E. coli* DNA photolyase, whose three dimensional structure is very well known, the most studied enzyme among its family members, was selected to conduct molecular docking simulations. Ligands for docking experiments were considered from U.S. Food and Drug Administration (FDA) approved drugs whose database is Super Drug Database with 2396 compounds (http://bioinformatics.charite.de/superdrug)

Although there is growing number of molecular docking software using different methods, docking simulations were performed via the most cited docking software, AutoDock and GOLD (Genetic Optimization for Ligand Docking) which have proven to be an effectively tool capable of quickly and accurately predicting bound conformations and binding energies of ligands with macromolecular targets [8-10]. In this study, two scoring functions are employed: AutoDock, and scoring function of GOLD, GoldScore Fitness. GoldScore Fitness is a force field based; AutoDock is a hybrid of both force field and empirical scoring functions [9, 10].

In this chapter, first, principles of AutoDock and GOLD are introduced with docking setup. Then computational results from automated docking simulations are presented and discussed.

2.2 AutoDock

AutoDock is freely distributed software developed to predict how small molecules bind to a target protein of known three dimensional structures. In this thesis, the latest version, AutoDock 4.2 is used.

In AutoDock 4.2, semi-empirical free energy force field is used to evaluate conformations during docking simulations. This force field is optimized for the system of large number of protein-inhibitor complexes to estimate both structure and inhibition constants, K_i. Free energy of binding is calculated by the sum of intramolecular energy changes in ligand and protein through binding, and plus intermolecular energy changes between ligand and protein through binding [11]. This equation is formulated below:

$$\Delta G = (V_{bound}^{L-L} - V_{unbound}^{L-L}) + (V_{bound}^{P-P} - V_{unbound}^{P-P}) + (V_{bound}^{P-L} - V_{unbound}^{P-L} + \Delta S_{conf})$$

(Eq 2.1)

In the free energy force field (Eq 2.1), there are six pair-wise energy evaluations (V) where P refers to protein, L refers to ligand and an estimate of conformational entropy loss upon binding (ΔS_{conf}) [12].

AutoDock uses a grid-based method for evaluation of the binding energy of different conformations in order to create large conformational space for a ligand around a protein. In AutoGrid, target protein is stored in a grid, and then a probe atom is sequentially placed at each grid point. In each grid point, the value of interaction energy between probe and target is stored [13]. Docking simulation is performed as a search for best conformations of ligand bound to target protein. AutoDock offers various conformational search methods such as stimulated annealing search method, traditional genetic algorithm and Lamarckian genetic algorithm.

Since Lamarckian genetic algorithm is a local hybrid of static and global stochastic methods, it offers most efficient searching methods for high degrees of freedom. Briefly, this algorithm creates a population of trial ligand conformations whose mutated generations looking for local minima with lowest binding energy [14]. Therefore, it is widely used and suggested by

producers of AutoDock, in this study Lamarckian genetic algorithm is employed as conformational searching method.

2.2.1 Using AutoDock

AutoDock docking process starts with employing 4 input files: PDBQT file for macromolecule, PDBQT file for ligand molecules, GPF file for grid parameters, and DPF file for docking parameters.

E. coli DNA photolyase was chosen as target protein as Sancar (1994) studied (see Figure 2.1 for representation of the protein in Accelrys Discovery Studio 2.5) [15,16]. PDB file containing three dimensional crystal structure of the target protein was downloaded from Protein Data Bank (www.pdb.org), as 1DNP.pdb. Next, via AutoDock Tools, this PDB file was converted to PDBQT file and applied Gastieger charges which is electrostatic model for each molecule and polar hydrogen atoms [17].
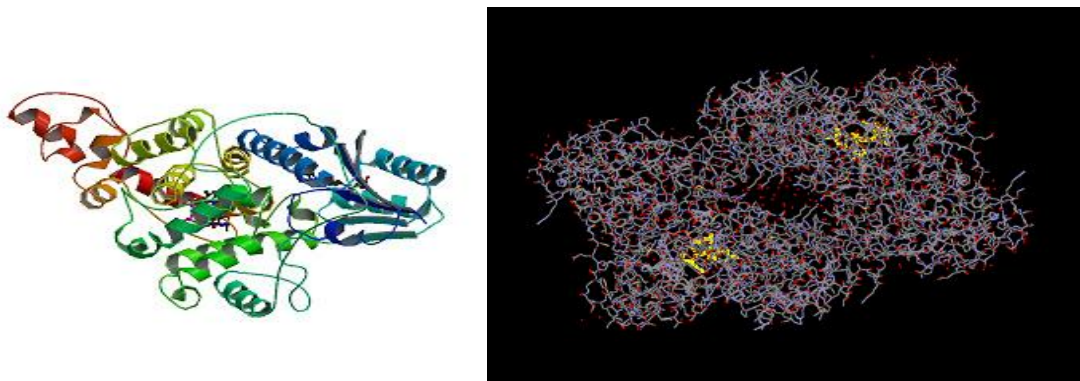
Figure 2.1 Experimentally determined crystal structure of *E. coli* DNA photolyase, 1DNP

Ligand molecules from SuperDrug Database were drawn in ChemDraw, then converted to three dimensional structures with minimized energy conformation by ChemBio3D Ultra 11.0 and saved in PDBQT file format (Figure 2.2).
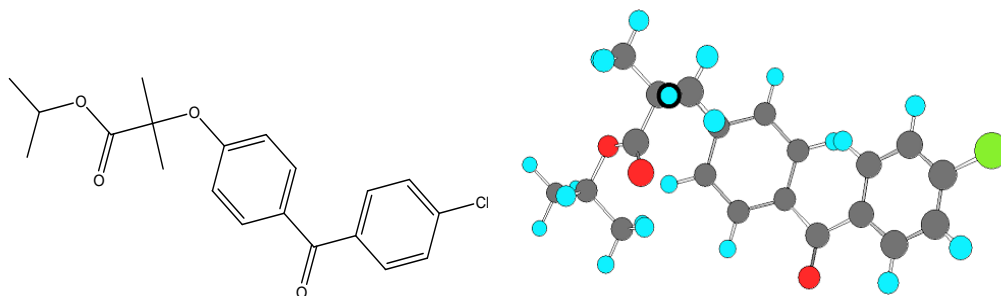
Figure 2.2 ChemDraw (left), ChemBio3D (right) representation of Fenofibrate

Subsequently, grid parameter file (GPF) was created via AutoGrid. In this file, grid center, grid size, spacing between grid points and the number of grid files are specifically defined in terms of atom types. In this thesis, grid center as the center of docking was decided to be "*FAD region of DNA photolyase, FAD472 residue of 1DNP*". Since catalytic activity of electron transfer occurs through the end of 6th nitrogen atom of FAD, N6 atom FAD472 (x,y,z coordinates of 26.051, 28.850, 40.506) was centered with partial charge of -0.0661. Grid size was adjusted as big as possible in order to see possible docked conformations over the region out of FAD472 region. Thus, maximum number of grid was specified as 60 x 60 x 60 with a default grid spacing 0.375 Angstrom (Figure 2.3).
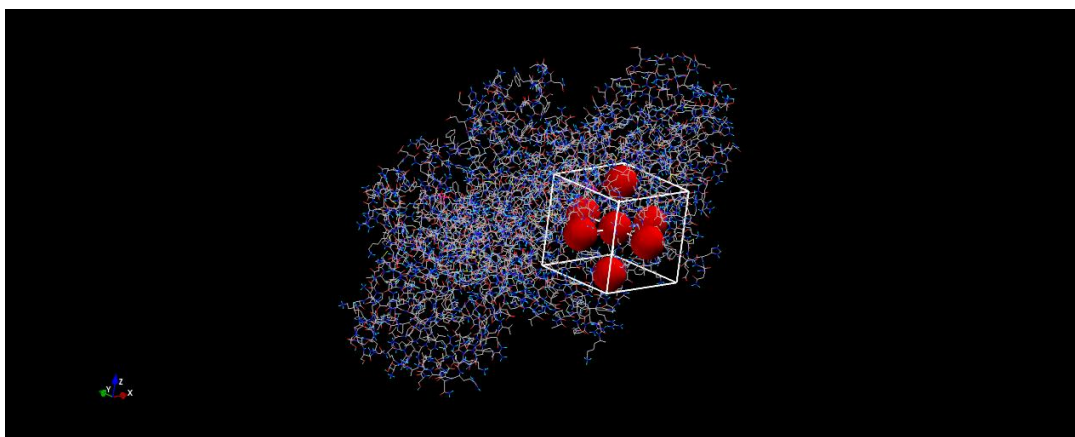
Figure 2.3 AutoGrid representation of DNA photolyase, 1DNP

Docking parameter files, DPF, was necessary to define docking parameters. Due to nature of this study, computational complexity and time consumed in virtual screening kept minimal. Thus, docking parameters were specified Lamarckian genetic algorithm with population size of

150, number of evaluations as 250,000, number of generations as 27,000, rate of mutation as 0.02, rate of crossover as 0.8. Number of run was 10-100. Sample docking parameter file, DPF is included in Appendix A1.

Automated docking simulations of 2396 compounds from SuperDrug Database on rigid DNA photolyase, 1DNP.pdb were performed with virtual screening software PyRx [19]. As a result of docking simulations, docking log files (DLG) give the prediction of structural conformation and kinetic parameters of binding/docking free energy.

2.3 GOLD

GOLD is automated ligand docking tool which uses genetic algorithm to simulate flexible ligand binding into the active site of the protein. Automated prediction of small molecules binding to protein is obviously a challenging task. GOLD producers affirm that GOLD has been tested with large number of complexes and GOLD solution was correct in %60-80 of experiments [20]. GOLD consists of three main parts: 1 – a scoring function which ranks different binding modes in accordance with protein-ligand hydrogen bond score, protein-ligand Van der Waals score, intramolecular hydrogen bonds in the ligand and intramolecular strain in the ligand. 2 – fitness of ligand in the binding site, 3 – a search algorithm to determine possible binding modes which modify dihedrals of ligand rotatable bonds, ligand ring geometries, dihedrals of protein OH groups and NH_3^+ and the mappings of fitting points. In this thesis, GoldScore Fitness was used as a scoring function. The GoldScore Fitness function is made up of four components: protein-ligand hydrogen bond energy (external H-bond), protein-ligand van der Waals (vdw) energy (external vdw), ligand internal vdw energy (internal vdw), ligand torsional strain energy (internal torsion) [21]

GoldScore Fitnesss function has been optimized for the prediction of ligand binding positions. It gives dimensionless number thus the prediction of binding affinities and kinetic parameters cannot be calculated, although some correlation between binding affinity and GoldScore Fitness has been found [20-21].

All docking simulations were carried out using standard default settings with FAD472 of rigid 1DNP as center of docking, a population size of 100, a maximum of 100 000 operations, number of islands as 5, a niche size of 2, and a mutation and crossover rate of 95.

2.4 Results and Discussion

The computational approach of this thesis relies on finding high binding affinity and selectivity of interactions between ligand/drug and active site of DNA photolyase /cryptochrome family proteins (FAD region). With this approach, it is desired to make a preliminary step to discover an interaction of an existing drug with photolyase, which can be used to inhibit/regulate the family proteins. Although there is strong research interest on these family of proteins, structure and mechanism of these proteins are not very well known yet, especially in terms of inhibition and regulation of these proteins. Successful reversible inhibition of these proteins may result in regulating functions of these enzymes such as DNA repair mechanism, circadian clock regulation. In the literature, there are two major studies focusing on inhibition of DNA photolyase; first, the study of DNA repair inhibition by caffeine (Sancar et al., 1990) which shows caffeine specifically binds to the damaged site of DNA and inhibits specific binding of DNA photolyase on CPD site of DNA [23]. Second method is based on ultraviolet light irradiaton to inhibit DNA photolyase activity [24]. In addition, there are some studies on regulation of circadian clock which refer to the interaction of human cryptochrome (CRY-DASH) specifically with another enzyme called phosphotase (PP5, PP7) [25,25]. However, none of these studies directly target photolyase protein itself. They only focus on their activity since mechanism of these protein structures are not well known yet. In addition, there is no computational molecular docking study found in the literature regarding kinetic analysis of interactions between photolyases and small biomolecules. Consequently, in this thesis, computational molecular docking approach was utilized in order to find a suitable drug to specifically bind to the bioactive site of DNA photolyase.

The structure based drug discovery approach may reveal direct inhibition process not only on DNA photolyase but also other family members due to homologous FAD region. Park et al. asserts that in addition to functional FAD residue, most of residues which interact with FAD are conserved for all eight known sequences of photolyases from microorganisms (see Table 1.1 for

microorganisms). These residues are only small subset of conserved residues in FAD binding domain [27-30]. They are TYR222, THR234, SER235, ASN341, ARG344, ASP372, and ASN378 (see Figure 2.5 for structural representation of FAD binding domain of *E.Coli* Photolyase (1DNP) in 3d molecule visualizing software, Accelrys Discovery Studio 2.5) Different colors represent different elements in Accelrys Discovery Studio 2.5; most common elements are colored as following:

Gray – Carbon (C), Soft Blue – Nitrogen (N), Red – Oxygen (0), Green – Chloride (Cl), Orange – Sulphur (S). See Appendix A2.1 for other elements, if needed.

The structure of FAD binding domain is an important detail to be analyzed for structure based drug discovery. As can be observed in Figure 2.4, catalytic cofactor FAD is non-covalently bound to protein but very tight in a U-shaped conformation with the isoalloxazine and adenine rings in close proximity to the domain surface. It is accessible to the flat surface of the protein through a hole in the middle of the domain. The size of the hole does not allow the diffusion of FAD in and out of the enzyme but has right dimensions and polarity to allow the entry of thymine dimer within van der Waals contact distance (2,5-4,5 Å) to isoalloxazine ring of FAD. The residues around the hole are hydrophobic on one side, polar on the other. [27-30].

It should also be noted that some residues have structural importance for photolyase activity of DNA repair. When photolyase specifically binds to a thymine dimer, residues ASN273, GLU274, and ASN341 have polar interactions with a thymine dimer. In addition to isoalloxazine ring of FAD, residues TRP277, TYR281, and TRP384 are also located in van der Waals contact with a thymine dimer. This mode of binding allows DNA repair activity [27-30].

Furthermore, Li Y.F. et al. found out that TRP277 plays crucial role in specific binding to CPD by examining site specific mutation on residues TRP277 with non-aromatic ring [31]. Park et al. (1995) also conducted site specific mutations on residues TRP277, TRP306 and showed that they involve electron transfer mechanism during DNA repair activity [27].
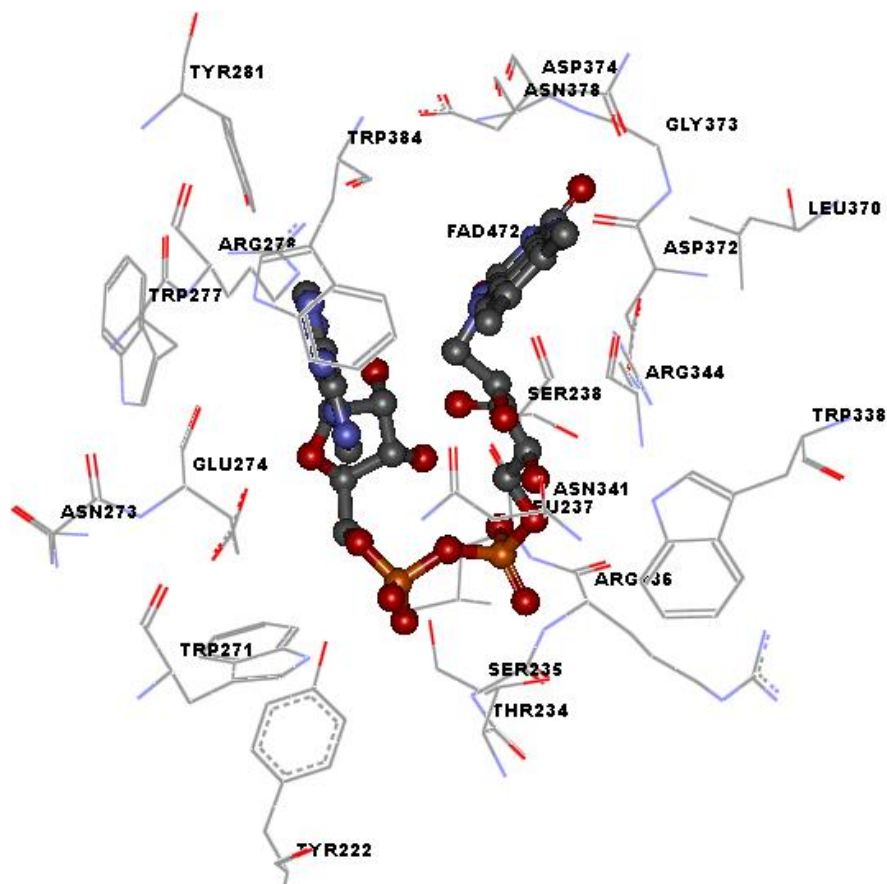
Figure 2.4 Residues close to FAD binding domain of *E.Coli* Photolyase, 1DNP.

(TYR222, THR234, SER235, ARG236, LEU237, SER238, TRP271, ASN273, GLU274,

TRP277, ARG278, TYR281, TRP338, ASN341, ARG344, LEU370, ASP372, GLY373,

ASP374, ASN378, TRP384, FAD472 – stick and ball)
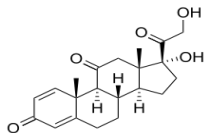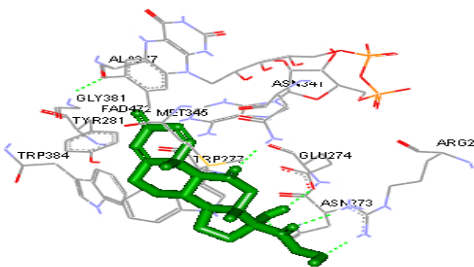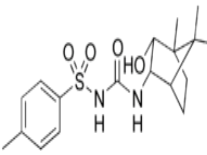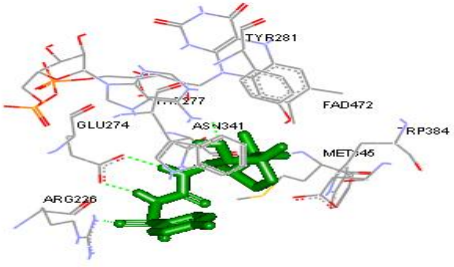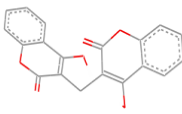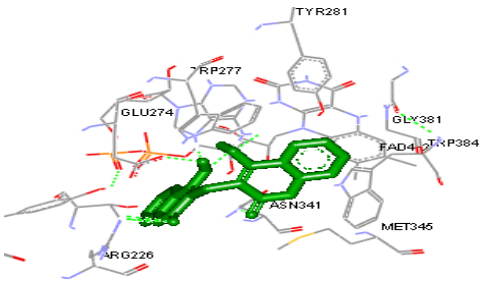
In this thesis, structure based approach suggests a drug candidate which is small enough (200-500 Da) to get into the hole of FAD region and form energetically stable complex. For this reason, small ligands for docking experiments were considered from FDA approved drugs whose database is Super Drug Database (http://bioinformatics.charite.de/superdrug) with 2396 compounds. As discussed before, *E. coli* DNA photolyase (1DNP) was selected to conduct molecular docking simulations with center of docking, FAD472 residue of 1DNP.
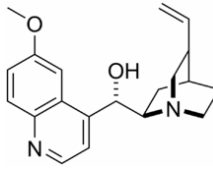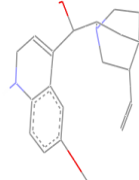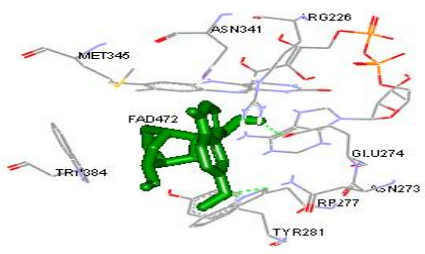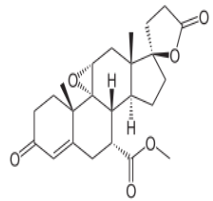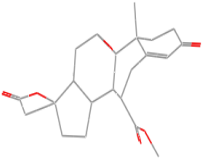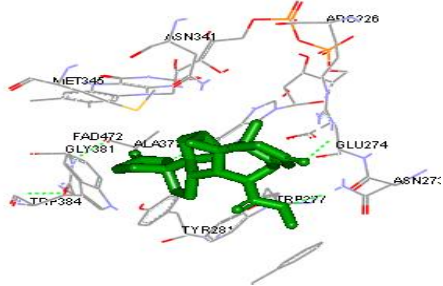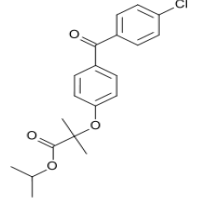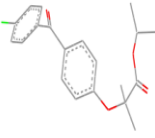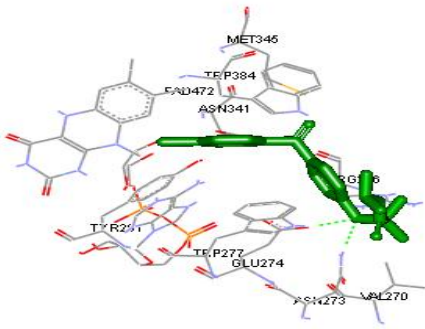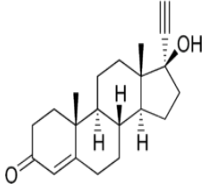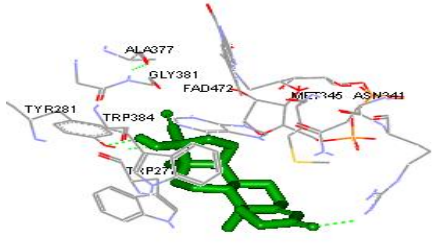
Virtual screening of docking simulations has been done, and then among 2396 compounds only 20 drugs are shortlisted in terms of results from AutoDock and GoldScore Fitness and availability in local pharmacy store. AutoDock was used to calculate the lowest

binding free energy whereas GoldScore Fitness gave dimensionless number which is used for prediction on how well ligand fits the binding position rather than prediction of binding affinity. Highest score of GoldScore Fitness is desirable. Fifty and above are considered as quite well score while 30-50 are considered as good score in GoldScore Fitness calculations, although there is no reliable scale for scores in the literature and supplemented by GOLD producers. Verdonk M.L. et al. claims that success rate for drug-like compound in GoldScore is up to %78, while this number is 60-70% for GOLD producers [20-21].
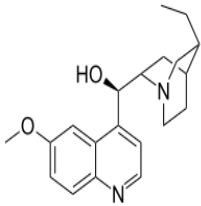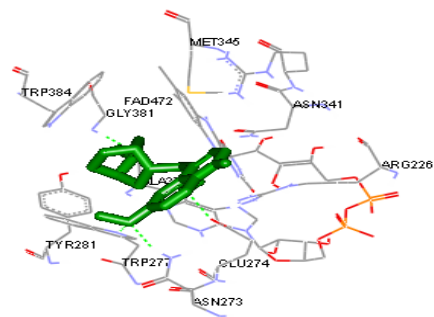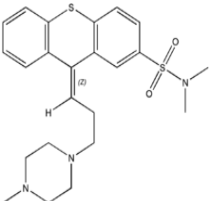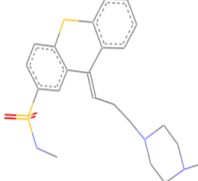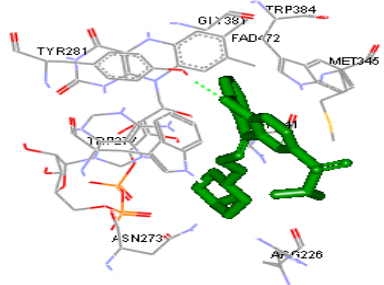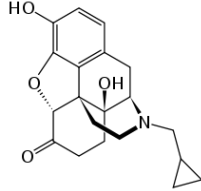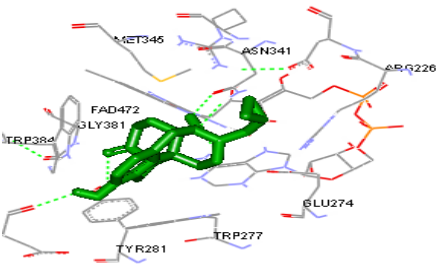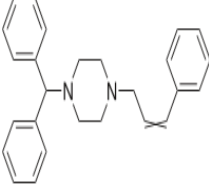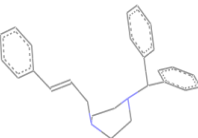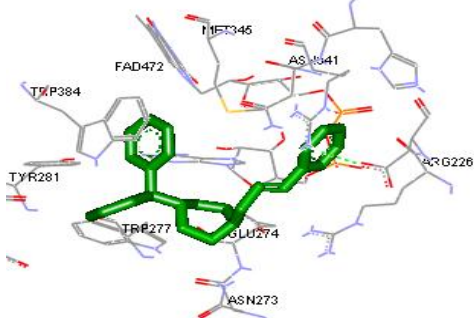
In Table 2.1, first column presents ligand Anatomical Therapeutic Chemical Classification System (ATC) Code, ligand name and ligand structure. Second column has two parameters of AutoDock results; first, estimated free energy of binding (ΔG) and its conversion to estimated inhibition constant, K_i (by the equation of $K_i = \exp(\Delta G /(R*T))$), and dimensionless GoldScore Fitness score. Third column gives ligand conformation after docking experiments. The last, fourth column shows the docked conformation of ligand (green structure) with close residues of DNA photolyase.

Table 2.1 Results of molecular docking for shortlisted 20 drugs. AutoDock results consist of two parameters: FEB: free energy of binding (kcal/mole), K_i: inhibition constant (µM)

ATC Code Drug Candidate	1. AutoDock FEB & K_i 2. GoldScore Fitness	Ligand Structure	Docked Conformation Residues Close to Ligand
A07EA03- Prednisone	-8,87 kcal/mole 0,316 µM 22 – 49		
A10BB04- Glibornuride	-7,90 kcal/mole 1.63 µM 35 – 47		
B01AA01- Dicoumarol	-7.70 kcal/mole 2.36 µM 46 – 55		

C01BA01- Quinidine	-8.20 kcal/mole 1.95 μM 46 – 57		
C03DA04- Eplerenone	-9.05 kcal/mole 0.231 μM 45 – 54		
C10AB05- Fenofibrate	-6.15 kcal/mole 30.58 μM 48 – 56		
G03DC04- Ethisterone	-8.13 kcal/mole 1.09 μM 31 – 39		

G03GB02-Clomifene	-5.95 kcal/mole 43.23 µM 31 – 37		
M01AC05-Lornoxicam	-6.92 kcal/mole 8.52 µM 56 – 58		
M01AH02-Rofecoxib	-7.93 kcal/mole 2.52 µM 46 – 54		
M01AH04-Parecoxib	-8.49 kcal/mole 0.599 µM 42 – 60		

M09AA01-Hydroquinine

-7.53 kcal/mole

3.03 µM

51 − 59

N05AF04-Tiotixene

-8.14 kcal/mole

2.19 µM

32 − 57

N07BB04-Naltrexone

-7.86 kcal/mole

1.75 µM

34 − 50

N07CA02-Cinnarizine

-7.92 kcal/mole

1.57 µM

37 − 56

P03BA02-Cypermethrin	-5.46 kcal/mole 99.95 µM 44 − 68	
R06AE05-Meclozine	-8.17 kcal/mole 1.03 µM 43 − 51	
R06AX19-Azelastine	-8.41 kcal/mole 0.687 µM 38 − 55	
R06AX27-Desloratadine	-8.76 kcal/mole 0.426 µM 29 − 48	

R06AX28-   -8.14 kcal/mole
Rupatadine   1.08 µM

                         37 – 58
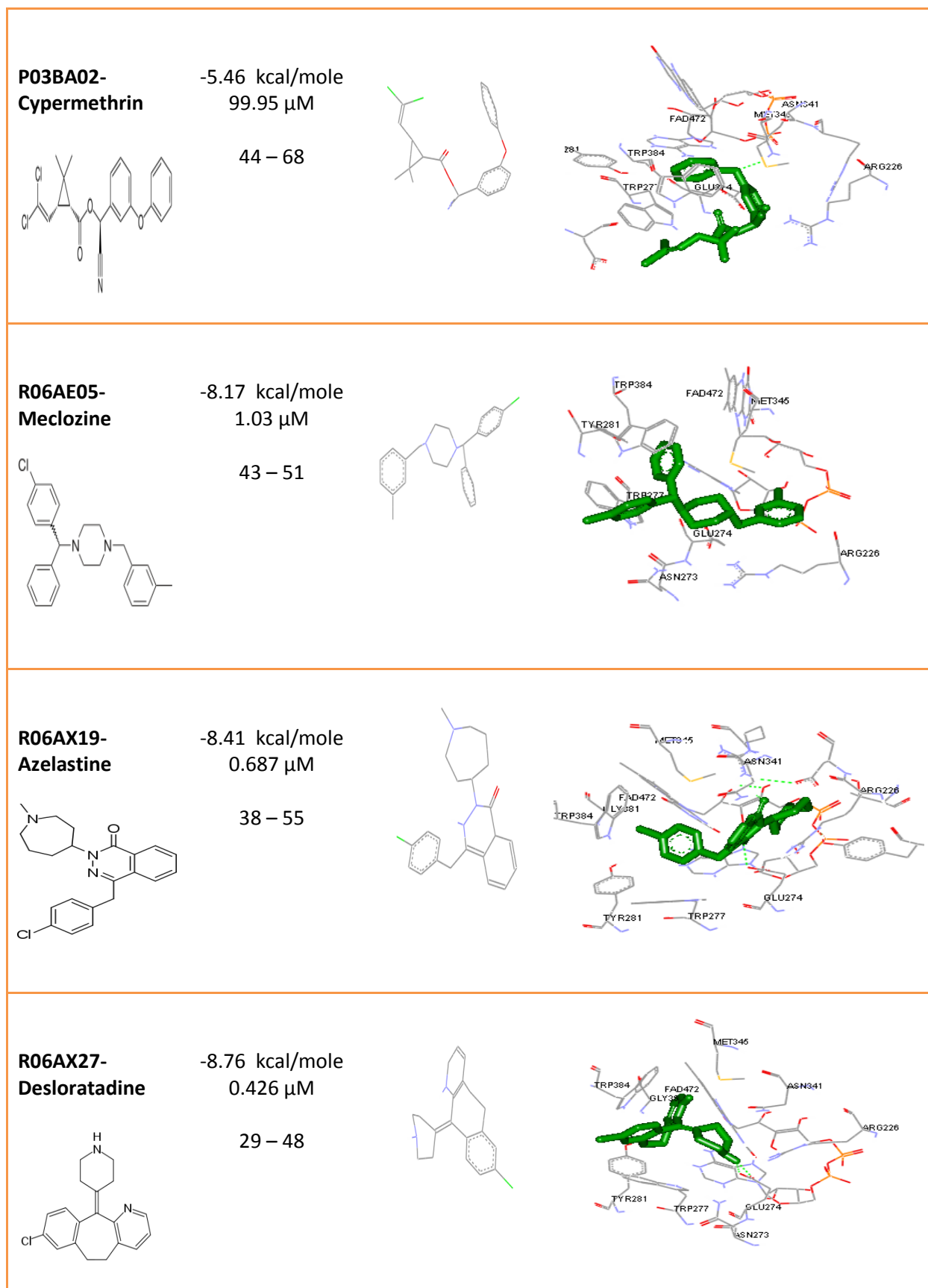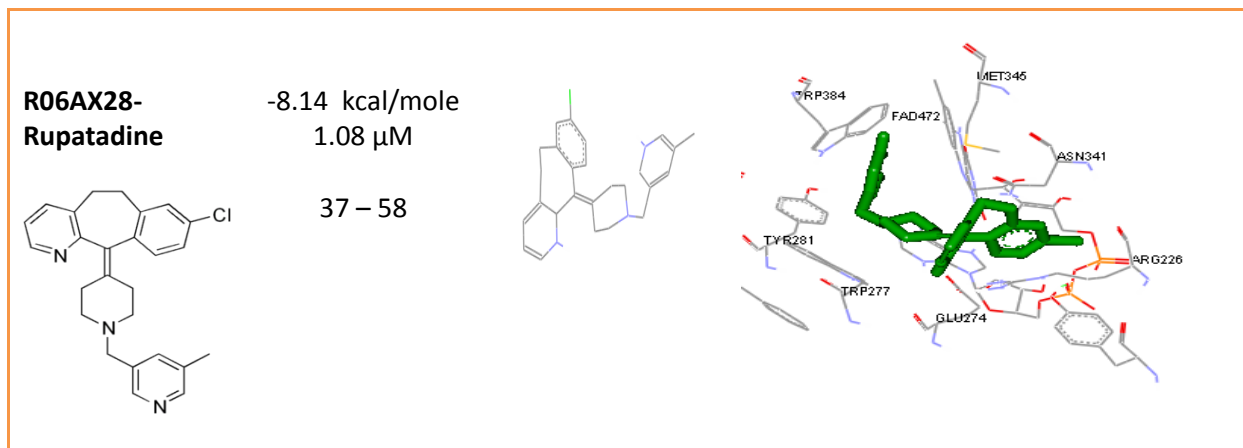
Results of molecular docking may reveal some common patterns for drug binding on FAD region. In this section, some findings of molecular docking is proposed and reviewed.

- FAD region was found as binding site of the *E.Coli* DNA Photolyase

Although many scientists found out FAD region was an active site of the photolyase enzyme, binding site for small molecules or drugs might be controversial since there is no study examining photolyase/drugs interaction. In this study, 2396 small compounds were docked to photolyase and almost all of them bind to FAD region in lowest free energy conformation as seen in shortlisted compounds (see Table 2.1). In order to analyze whether drugs can specifically bind other side of the photolyase, the docking area (grid area) was kept maximum as 22.5 x 22.5 x 22.5 in Angstrom (Å) grid spacing where dimensions of *E.Coli* DNA photolyase are 62.60 Å, 72.20 Å, 58.50 Å. In addition, blind docking was randomly done on different regions of photolyase but there is no considerable binding seen. Shortly, this finding validates the preliminary but important step as FAD region is the binding site for these drug candidates.

Drugs with molecular masses smaller than 300 Da and larger than 450 Da do not specifically bind to FAD region. As discussed earlier, in order to ensure stability of non-covalently bound FAD in the enzyme, FAD residue is deeply buried and accessible to the flat surface of the protein through a hole in the middle of the domain. The size of the hole does not allow the diffusion of FAD in and out of the enzyme. In accordance with the

small size of the binding domain, findings of the study show that molecules above 450 Da have higher free energy of binding and the larger the drug, the higher the free energy of binding is. Also, among the lowest energy conformations, there is no drug compound less than 300 Da.

These findings are also suitable with famous "Lipinski Rule of Five" describing molecular properties important for a drug's pharmokinetics in human body. Lipinski rule claims that an active drug has no more than one violation of the following criteria: a molecular mass from 160-500 Da, not more than 5 hydrogen bond donors, not more than 10 hydrogen bond acceptors, an octanol-water partition coefficient, log P not greater than 5 [32].

- When drugs from Table 2.1 are analyzed in terms of their sub-structures, some common patterns come out, as the presence of some groups are important for binding interactions between drug and photolyase. These sub-structures are mainly *6-membered aromatic, heterocyclic compounds and aryl derivatives*.

  ✓ 6-membered cyclic compounds – benzene, piperidine, piperazine, pyridine (Figure.2.5)
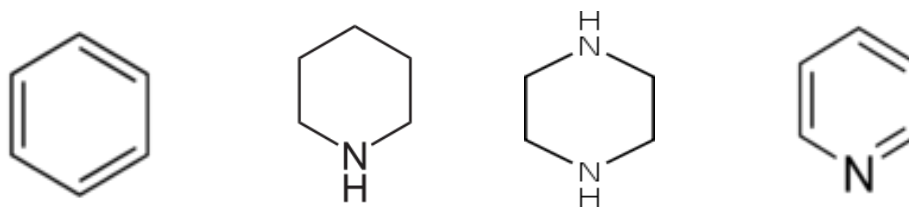
Figure 2.5 benzene, piperidine, piperazine, pyridine (left to right)

  ✓ Aryl derivatives – phenyl, phenylpropenes, phenols (Figure 2.6)
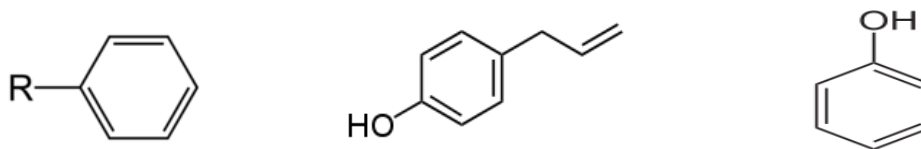
Figure 2.6 Phenyl, phenylpropenes, phenols (left to right)

- Drugs with 3-4 cyclic ring structures have higher binding affinity on photolyase.

Top 2 lowest free binding energy conformations, Eplerenone (-9.05 kcal/mole) and Prednisone (-8.87 kcal/mole) are steroid derivatives whose structures involve 4 fused cycloalkene rings. Almost all of compounds in Table 2.1 contain 3-4 cyclic rings, especially aromatic rings consisting of benzene and pyridine structures.

The positive effect of ring structures in binding may be reviewed in accordance with the structure of FAD binding domain. As implied before, in order to keep catalytic cofactor, FAD attached in the protein, surface of the FAD domain is conserved with aromatic hydrophobic groups (especially TRP residues). In Figure 2.7, dominancy of hydrophobic groups (white) around the hole leading to FAD472 residue is highlighted with a square mark.
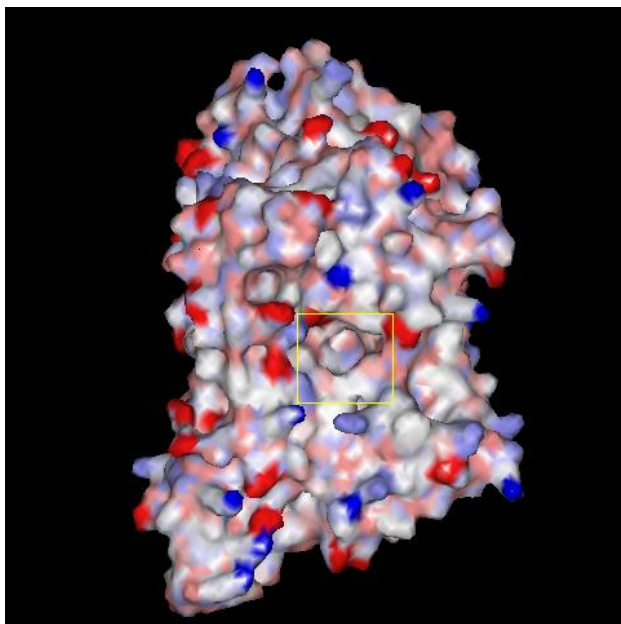
Figure 2.7 Surface potential representation of 1DNP residues. Blue represents basic groups; red, acidic groups; white, hydrophobic groups. The square marks the hole leading to FAD472 residue.

Therefore, in order to interact with FAD region, a drug should avoid limitations on polarity of the domain as to have hydrophobic aromatic rings in its structure.

- Drug candidates make hydrogen bonding mostly with specific residues of the binding domain: ARG226, ASN273, GLU274, TRP277, ASN341, and FAD472.

Hydrogen bonding, like any other bonding, provides binding energy to the protein-ligand complex. In structure based drug discovery approach, ligand is not covalently bound to the target protein, so contribution of hydrogen bonding to the free energy of binding is quite high. In Table 2.1, the last column gives docked conformation of the drug in the binding domain with close residues. Green dash lines between drug's atom and residue atom represents hydrogen bonding. Detailed list of hydrogen bonds in binding for each drugs are given in Appendix A3.

As can be observed in Table 2.1, residues close to the binding sites are almost identical for each ligand binding. In addition, hydrogen bonds were formed between oxygen atoms of drugs' side chains and hydrogen atoms of binding domain residues: ARG226, ASN273, TRP277, ASN341 and FAD472.

ARG and ASN are amino acids with polar neutral side chains and quite hydrophilic, thus this fact can explain why most of the binding predictions include ARG226, ASN273, and ASN341 as hydrogen donor to the oxygen atoms of the drugs' side chains. As shown in Figure 2.5, ASN273 and ASN341 were found out as residues closest to FAD472, functioning site of the photolyase. Studies also show that ASN273 and ASN341 were needed in creating specific binding cavity for CPD binding during DNA repair process. The finding that drugs form hydrogen bonding these residues can be also applied to other photolyase family of proteins since these residues are also conserved in other family members [27-30].

TRP277 was also identified as crucial residue in photolyase activity both in specific binding cavity and electron transfer mechanism during redox state of DNA repair. Hydrogen bonding with crucial residue of the photolyase, TRP277 may be an important tool in inhibiting/regulating the enzymatic activity of photolyase since this bonding can create reversible changes in both structure and electron transfer pathway of the residue TRP277. Again, this residue is also conserved in other family of proteins.

Another important finding is hydrogen bonding with FAD472 residue which is functioning side of the enzyme. Length of hydrogen bonding varies from 1.6 Å to 2.4 Å. In most of the cases, hydrogen bond was formed between oxygen atom of the drug and hydrogen atom attached to nitrogen backbone of the FAD472 (N6) where the catalytically active atom of FAD472 is in redox state of electron transfer pathway. N-H…:O bond strength is approximately 1.9 kcal/mole, although it varies with bond length, geometry, temperature, etc. [33]. In short, existence of hydrogen bonding of drug candidates and FAD472 may be a fundamental occurrence in direct inhibition of the photolyase enzyme.

Last considerable pattern in hydrogen bonding is with GLU274 residue. As ASN, ARG residues discussed above, GLU274 is also in polar interactions with thymine dimer and functional in creating specific binding cavity. Like ASN and ARG aminoacids, GLU is also hydrophilic and it has polar neutral side chains. In contrast to ASN and ARG residues, GLU277 interacts with drug candidates as hydrogen acceptor. This interaction can be explained by the fact that GLU has both hydrogen donor and acceptor atoms in its side chains.

- Among 2396 FDA approved drugs; Eplerenone has the lowest binding free energy conformation on FAD region of DNA photolyase.

Among 2396 compounds from, Eplerenone has the lowest binding free energy conformation with DNA photolyase (-9.06 kcal/mole, 231nM). Although, GoldScore Fitness result for best fit conformation of Eplerenone binding, 54, is not the best score (preferably above 60) but in the literature, this score is acceptable due to its appropriate binding position. It should be restated that GoldScore Fitness does not support information about binding affinity but gives fitness score indicating stability, feasibility of drug's binding position. In addition to Eplerenone's success in scoring functions, this drug candidate is very well positioned in docked conformation since it directly interacts with crucial residues of enzyme which are responsible in enzymatic activity. Docked conformation of Eplerenone in binding domain can be seen in Table 2.1 with green dash which represents hydrogen bonding between an atom of eplerenone and corresponding atom of the residue. Details are highlighted below:

Table 2.2 Hydrogen bonding sites of Eplerenone (as UNK0)

Hydrogen Bonding Sites	Distance (Å)
A:ARG226:HH22 - :UNK0:O	2.27306
A:ASN273:HD22 - :UNK0:O	2.28541
A:TRP277:HE1 - :UNK0:O	1.83643
A:FAD472:H6A1 - :UNK0:O	1.66298

Eplerenone forms 4 hydrogen bonds with 4 different residues as its hydrogen acceptor count is 4. Functionality and importance of these residues are just discussed in previous parts. Especially bond length with FAD472, 1.66 Å indicates the strength of the bonding (for ex. thymine dimer is bound to FAD region within 3Å − 3.5Å van der Waals contact distance to FAD472) [27].

2.5 Remarks

Successful drug candidates in this study possess a fundamental structural character which is the "*asymmetric polarity*". This asymmetric polarity exists in a suitable drug candidate which consists of both hydrophobic ring structures (3-4 rings) and polar structures having nitrogen and oxygen capable of forming hydrogen bonds. This proposal is also supported by the structural analysis which reveals that residues localized on the wall of the groove where FAD472 residue is conserved are hydrophobic on one side and polar on the other (see Figure 2.1 and [16, 27]).

In this thesis, with the computational approach used, screening for interactions between existing drug molecules and photolyase was successfully performed, and drugs with high affinity binding to photolyase FAD region were discovered. Although further computational works can be done especially in terms of lead optimization with different approaches as structure modifications, molecular dynamics, homology modeling, etc., the scope of this study was limited to FDA approved drugs and experimental validation of kinetic parameters of interaction between DNA photolyase and these drugs.

Chapter 3

Expression and Purification of DNA Photolyase

3.1 Expression and Purification of *E.coli* DNA Photolyase

In this part of study, *E.coli* DNA photolyase (EC 4.1.99.3) was expressed and purified in order to analyze biochemical interaction between DNA photolyase and potent drugs using Surface Plasmon Resonance (SPR). Following sections explain the basic methodology of expressing and purifying *E.coli* DNA photolyase.

3.1.1 Competent cell transformation

Plasmid pMAL was added (with inserted sequence of DNA photolyase) to 100 µl of competent cells *E. coli* (DH5α) and the mixture was kept on ice for 10 min, then transferred to water bath of 45 °C for 90 s. Heat shock enables formation of pores in cell membrane and uptake of plasmid [34]. After heat shock, mixture was kept again on ice for 1 min. LB Amp Glc broth in the amount of 900 µl (4 g LB, 200 ml water, 0.4 g glucose, 200 µl ampicillin (final conc. 1 µg/ml)) was added and the mixture was incubated at 37 °C for 30 min. Next, it was centrifuged for 6 min at 14000 rpm and resuspended in 200 µl of supernatant to concentrate cells in smaller amount of medium. Inoculation of agar plate should be always made with no more than 100 µl of cell culture. The mixture was then transferred as 2x 100 µl to 2 agar LB Amp plates (4 g LB, 3 g agar, 200 ml water, 200 µl ampicillin (final conc. 1 µg/ml)) and incubated over night at 37 °C.

3.1.2 Expression of DNA photolyase

INDUCTION OF EXPRESSION

First, one colony from LB Amp agar plate was transferred to 2 ml of LB Amp Glc culture medium, then was kept to grow at 37 °C over the night. Glucose in the culture medium was necessary to repress expression of bacterial amylase, which also has high affinity for amylose in the column and could degrade it. 200 ml of LB Amp broth was inoculated with 2 ml of overnight culture. Then culture kept at 37 °C until A_{600} reaches 0.5, which means the cell density is ~ 2×10^8 cells/ml. 1 ml of sample was taken to centrifuge it for 2 min at 14000 rpm and then stored at -20 °C. Then sample was to use for SDS PAGE (uninduced sample), resuspended in 10 µl of $2\times$ SDS PAGE sample buffer.

IPTG solution with a concentration of 1 M, in the amount of 60 µl(final concentration must be 0.3 mM) was added to the rest of the LB Amp Glc culture medium to induce expression of photolyase. IPTG was used to inactivate lac repressor, which binds to P_{tac} and prevents transcription of genes downstream P_{tac}. Without IPTG, expression of fusion protein MBP-photolyase was supposed to be low and enable cells to grow and divide faster until desirable cell density is reached.

Sample was kept to grow for 2 h at 37 °C. 1 ml of sample was taken to centrifuge for 2 min at 14000 rpm and stored at -20 °C. It was again used for SDS PAGE (induced sample), resuspended in 20 µl of SDS PAGE sample buffer. Comparison of uninduced and induced sample with SDS PAGE was needed to get information about the level of induction.

HARVESTING

During harvesting step it is important to keep samples on ice all the time to prevent degradation of protein. The rest of LB Amp Glc culture medium was centrifuged for 20 min at 4000 g and at 4 °C. Pellet was resuspended in 10 ml of column buffer. The sample was sonicated on ice in pulses of 15 s, altogether for ~2 min. During sonication step substantial amount of heat is released, therefore it is crucial to perform sonication on ice and have pauses between pulses.

Then, sample was again centrifuged for 30 min at 9000 g and at 4 °C. According to the protocol, supernatant (=crude extract) should be diluted to protein concentration of ~ 2.5 mg/ml. In most cases this means dilution 1:5 with column buffer. Since the amount of protein in case of photolyase was not high and dilution may cause denaturation of proteins, it was not necessary to dilute the protein. Dilution 1:3 or no dilution at all did not affect efficiency of the column purification.

Before dilution 10 µl of crude extract was taken for SDS PAGE (crude extract before purification). Column buffer (1 ml) was added to the pellet, resuspended and stored at 4 °C. It was used for SDS PAGE (insoluble matter). Comparison of insoluble matter, crude extract before purification and samples after purification on SDS PAGE indicated that purification was efficient. In case there is little or no protein after purification, sample of insoluble matter gives information about the amount of protein in inclusion bodies, so one can tell whether lack of protein is due to inefficient purification or formation of inclusion bodies.

In order to scale up the process, 10 ml of overnight culture was used and 1 L of LB Amp Glc culture medium was prepared. After 20 min centrifugation, pellet was resuspended in 50 ml of column buffer. Column buffer was prepared as 20 mM Tris HCl, at pH 7.4, 200 mM NaCl, 1 mM EDTA, and optional: 10 mM β-ME or 1 mM DTT (to prevent formation of intermolecular disulphide bridges), 1 mM sodium azide (bacteriostatic) and stored at 4 °C.

3.1.3 Purification

MBP-tagged proteins were purified on amylose resin by affinity chromatography according to the manufacturer's protocol (New England BioLabs Inc, NEB, England) [35-40]. Amylose column (binding capacity was 3 mg of protein/ ml of resin) was prepared. Three ml of amylose resin poured into the column and was kept until resin sinked to the bottom and then it was washed with 8 column volumes of column buffer. The crude extract was loaded with flow rate 10x (diameter of column [cm]) ^{2}/h. Then, it was again washed with 12 column volumes of column buffer, and eluted with 2 - 4 column buffers with 10 mM maltose. 12x1 ml fractions were collected and presence of protein was checked with Bradford reagent. Protein usually appeared in 3rd or 4th fraction.

Ten µl of sample was added to 1 ml of Bradford reagent in order to see if there was any change of color from brown to blue. Samples were stored where change of color occurs at -4 °C and 10 µl of those samples were taken for SDS PAGE (purified sample).In order to scale up, 15 ml column for 1 L of culture medium was used, and 15x1.5 ml fractions were collected. The presence of protein with Bradford reagent was checked as stated above. Protein usually appears in 7 – 10 fractions.

Scale up of elution buffer:

Column volume:	3 ml	15 ml
2-4 volumes column buffer:	12 ml	30 ml
10 mM maltose:	0.041 g	0103 g

Regeneration of column (at 4 °C):

Column was washed with 3 column volumes of water, 3 column volumes of 0.1 % SDS (make sure that solution was kept at room temperature until needed to prevent precipitation of SDS), then 1 column volume of water and 3 column volumes of column buffer.

SDS PAGE

For SDS experiments, 10 % running gel, 5 % loading gel were used. There were 5 samples:

1. Protein ladder

2. Uninduced cells: resuspend pellet in 10 µl 2x SDS PAGE buffer

3. Induced cells: resuspend pellet in 10 µl 2x SDS PAGE buffer

4. Crude extract: 10 µl of sample + 10 µl of 2x SDS PAGE sample buffer

5. After purification: 10 µl of sample + 10 µl of 2x SDS PAGE sample buffer

Samples were added in boiling water for 5 min to lyse the cells and denature proteins. Ten µl of sample was loaded on SDS PAGE gel. Then they ran at 80 V for loading gel and 160 V for

running gel. Figure 3.1 presents strong band in lane 5 indicating the presence of DNA photolyase – MBP (nearly 85 kDa)
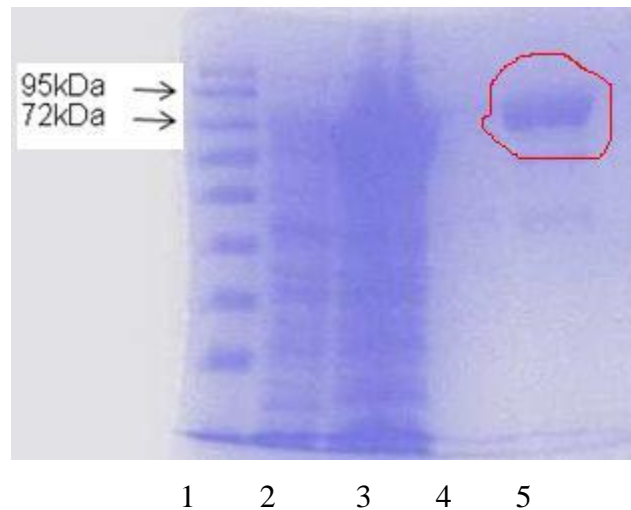
Figure 3.1 Expression and purification of DNA Photolyase - MBP

Determination of the concentration of purified protein

In order to determine the concentration of purified protein, Bradford assay was used. BSA (1 mg/ml) was used as a standard in the experiment. Ten µl of sample was added to 1 ml of Bradford reagent. Absorbance was measured at 595 nm and then standard curve was obtained to determine protein concentration in fractions (Figure 3.2). From the standard curve, mass of 4 samples were calculated. And finally total concentration of purified protein was calculated as 7.72 mg protein in 2.4 ml buffer which corresponds to 3.21 mg/ml (Table 3.1). Absorbance and concentrations data for both BSA and sample are provided in Appendix A3.
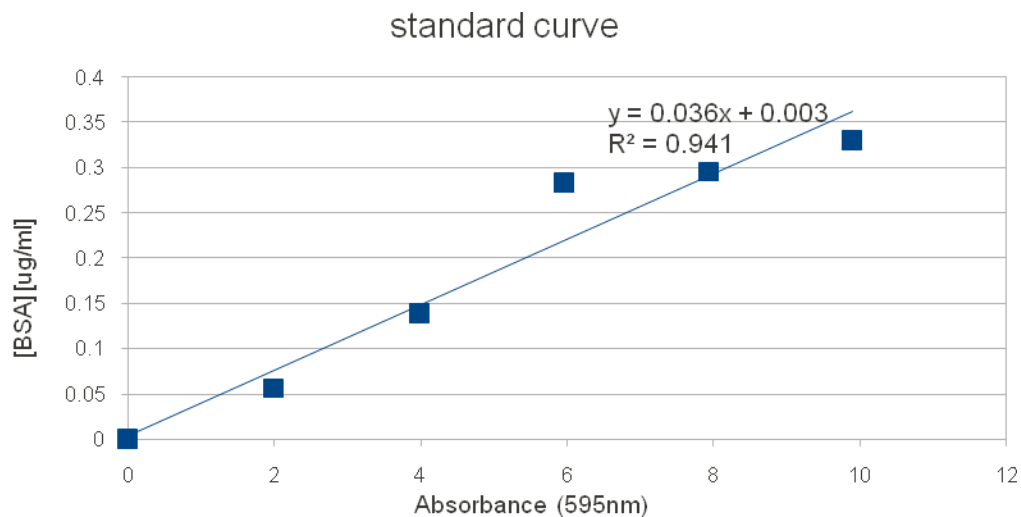
Figure 3.2 Determination of concentration with Bradford Assay

Table 3.1 DNA Photolyase-MBP mass determination

Sample	V (culture medium) [ml]	m (sample) [mg]
1	200	2.14
2	200	0.83
3	1000	2.36
4	1000	2.38
Total		**7.72**

Dialysis & Storage Buffer

In order to store protein for extended periods oftime, it is necessary to change the column buffer with storage buffer containing glycerol which prevents freezing, so that the sample could be stored at -20 °C. Storage buffer consists of 50 mM Tris HCl, pH 7.5, 100 mM KCl, 1 mM EDTA, 5 mM DTT, and 50 % glycerol. Samples were transferred into activated dialysis membrane and bound it tightly to prevent leaking of the sample, and then overnight dialysis was performed. Finally, sample was transferred to the new tube and stored at -20 °C.

3.2 Biotinylation of *E. Coli* DNA photolyase

E.Coli DNA photolyase was biotinylated for its further immobilization on avidin functionalized sensor surface of SPR. Biotin and avidin has strong affinity with a binding constant, K_D of 10^{-15}, and this affinity have been utilized extensively in biological assays [40].

The most common target for modifying protein molecules is the amine group which is abundant in lysine (LYS) amino acid. As an amine reactive biotinylation reagent, NHS-Biotin reagent (purchased from Uptima, USA) has been used in this study which is essentially insoluble in water. Since reactions will be in aqueous solution, they must be first dissolved in an organic solvent, then diluted into the reaction buffer, running buffer. The most commonly used organic solvents for the purpose are DMSO and DMF, whose concentrations up to 6-8 % are compatible with most of the proteins.

Dialysis of DNA photolyase Storage Buffer:

Since Tris has primary amine group Figure (3.3), it may interfere with NHS conjugation of photolyase. Thus, Tris based storage buffer for photolyase (50 mM Tris Hcl, pH 7.5, 100 mM KCl, 1mM EDTA, 5 mM DTT, 50 % glycerol) was dialyzed against PBS buffer according to the following procedure:

Fifty µl storage buffer was diluted with PBS to 1 ml in an eppendorf tube. Dialysis buffer (400 ml of buffer in 50 mM HEPES, pH 7.5, 100 mM KCl, 1mM EDTA, 5 mM DTT, 50 % glycerol) was prepared, and overnight dialysis was conducted at $+4^o$ C.
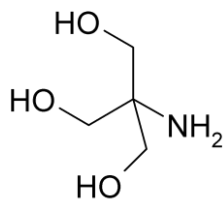
Figure 3.3 Molecular structure of Tris, $(HOCH_2)_3CNH_2$

Conjugation of Biotin-NHS and DNA photolyase

Photolyase protein was prepared at 0.7 µM in PBS (NaCl 150mM, Phosphate 20mM, pH7.5). Biotin-NHS solution was prepared at 10.5 mM in 400 µl anhydrous DMSO. Next, 400µl of biotin-NHS was added into 1 ml of protein solution at 0.7 µM. This solution was incubated at room temperature with constant mixing for 4 hours.

Dialysis after of Biotinylation

In order to remove unreacted biotin-NHS, special dialysis cassette with a molecular weight cutoff of 3500 Da is used. PBS in the amount of 1.2 L (NaCl 150 mM, Phosphate 20 mM, pH 7.5) was prepared. Slide-A-Lyzer Dialysis Cassette (with 0.5-3.0 ml capacity, 3500 MWCO) was used to dialyze the biotinylated conjugate. PBS solution containing biotin-NHS & Photolyase in the amount of 0.5 ml was dialyzed against PBS overnight at +4°C in 600 ml of PBS with frequent medium changes. Finally, the purified conjugate is stored at -20 ^{o}C for further use in SPR experiments.

Chapter 4

Characterization of Interaction via Surface Plasmon Resonance (SPR)

4.1 Analysis of biomolecular interactions

In a traditional drug discovery process, experimental screening of small molecules against a validated target protein was mainly explored by a static affinity assay format in which high affinity is employed as a selection criteria [41,42]. Demand on testing increasing number of compounds in drug industry require more sophisticated formats and high throughput assays to improve efficiency of the process in terms of complexity, time and money [43]. In biological environment, concentration of ligands change rapidly with binding/releasing reaction in milliseconds, thus the kinetics of interactions play an important role especially in structure based drug discovery process where competitive mode of binding occurs in a dynamic nature. To this end, Swinney's findings clearly reveal that biological potency was better described by the dissociation rate constant than by equilibrium binding affinity [44]. This can explain the increasing importance of non-equilibrium interaction kinetics analysis tools in the last decade of pharmaceutical industry.

SPR-based biosensors are nowadays most popular class of biosensors commonly applied in both research and pharmaceutical industry. Their features such as label-free detection, real time data analysis and ease of use make them well suited tool for biomolecular interaction analysis in drug discovery process [44]. In the industry, they are mainly used as secondary screen for validation purposes. In this thesis, Surface Plasmon Resonance (SPR) technology was applied to review kinetic analysis of DNA photolyase/drug interaction. More detailed explanations for SPR technology will be given in the later parts of this chapter.

There are also various techniques to determine binding affinity, kinetics, and thermodynamics of biomolecular interactions besides SPR. All have specific advantages and disadvantages, therefore all these techniques should not be considered as competitive but rather complimentary to each other. These methods are simply tabulated in Table 4.1 in terms of their specifications on different parameters of biomolecular interaction [46].

Table 4.1 Characterization methods for drug/target interaction

	Affinity	*Kinetics*	*ΔH ΔS*	*Stoichio-metry*	*Conformational Changes*	*Label Free*
SPR	✓	✓		✓	✓	✓
CD	✓				✓	✓
ITC	✓		✓	✓		✓
MPA	✓		✓			
NMR	✓					✓
SFS	✓	✓			✓	
AUC	✓			✓	✓	✓
DPI	✓	✓		✓	✓	✓

CD: circular dichroism,   ITC: isothermal titration calorimetry,
MPA: microtiter plate assay,   NMR: nuclear magnetic resonance,
SFS: stopped-flow spectroscopy,   AUC: analytical ultra-centrifugation,
DPI: dual polarization interferometry

4.2 Surface plasmon resonance

Surface plasmon resonance is defined as the excitation of surface plasmons by light. From the formal definition to practical applications of SPR as a monitoring tool for biomolecular interaction was first demonstrated in 1983 by Liedberg et al. [46] After invention of commercial SPR, SPR biosensors became a suitable tool to analyze kinetic and affinity parameters of ligand - analyte interaction based on refractive index change. SPR applications are conducted in various studies such as receptor-ligand interactions, antibody antigen interactions, conformational change studies and virus, especially HIV studies [47-53].

4.2.1 Theory of Surface Plasmon Resonance

Basic principles of SPR phenomenon are based on total internal reflection (TIR), evanescence electric field and surface plasmon waves. Total internal reflection occurs in thin conducting metal films at an interface between two media of different refractive indices (e.g. glass-air). When polarized light is in incident on the reflecting interface, change in electric field intensity generates evanescence wave. This wave is exponentially reduced with the distance from the surface and leaks from one medium to other. When the evanescence field passes through a thin metal film, electromagnetic surface plasmon waves are induced in the metal film. Plasmons are regarded as electron density fluctuations in a conducting metal. Gold is commonly used as a non-magnetic metal layer with a thickness lower than the wavelength of the incident light [54].

Both surface plasmons and photons are a form of electromagnetic energy whose properties can be simplified as the manner of vector quantities. The momentum of light in the interface can be resolved into two vector components as parallel and perpendicular to the interface. The magnitude of these vector components directly depend on the light angle [55]. The surface plasmon wave can also be represented with vector quantities as the light momentum. These vectors depend on various factors which affect momentum of plasmon waves; such as metal properties, layer thickness, surrounding media [56-58]. In order to make resonance phenomenon occur, photons should be converted into the form of plasmons, otherwise light is

fully reflected from the gold surface. This conversion happens only when the momentum of incident light vector exactly correspond to the one of the surface plasmon vector [55].

During the experiment, metal nature, thickness and properties of medium are kept constant so resonance conditions are only dependent of the angle of light incidence and the refractive index of the second medium. Therefore, changes in the medium can be monitored by adjusting the angle of light incidence until a resonance is reached [56-58].

SPR biosensors use this phenomenon to detect mass changes in a sample cell. A sensor chip carries a thin gold layer (50 nm) on a glass support. This gold surface is directly connected with flow cell and a glass prism. P-polarized light beam at 760 nm penetrates through glass prism and is internally reflected at the interface which then employs evanescence wave allowing refractive index change. By detector array, angle of light incidence continuously is detected. The angle at which intensity of reflected light passes through minimum corresponds to generation of surface plasmon resonance, and this causes a dip in the intensity of reflected light. This angle is called resonance angle or SPR angle [59]. During biomolecular interaction, absorption of molecule around the surface will change the refractive index of the medium which is monitored as the change in the angle of incidence light. This change is then converted to response signal which is represented as resonance unit (RU)

Among the SPR angle, 0.1° shift is equivalent to 1,000 RU, and for an average protein this corresponds to a surface concentration change of about 1 ng/mm^2 or in other words: 1 RU = 1 pg/mm^2 [60]. The correlation between RU and surface concentration may be different for non-protein species. Although there can be some minor deviations, it has been claimed that nucleic acids and protein have similar dependencies [2].

4.2.2 Steps of SPR Assay

In a typical SPR biosensor experiment, one target component is immobilized on the sensor surface at first. This component is called ligand. Then, a second component, analyte, is

injected in solution at constant concentration into the buffer flow to capture the immobilized component, and this complex formation on the sensor surface is monitored by detector array (Figure 4.1).
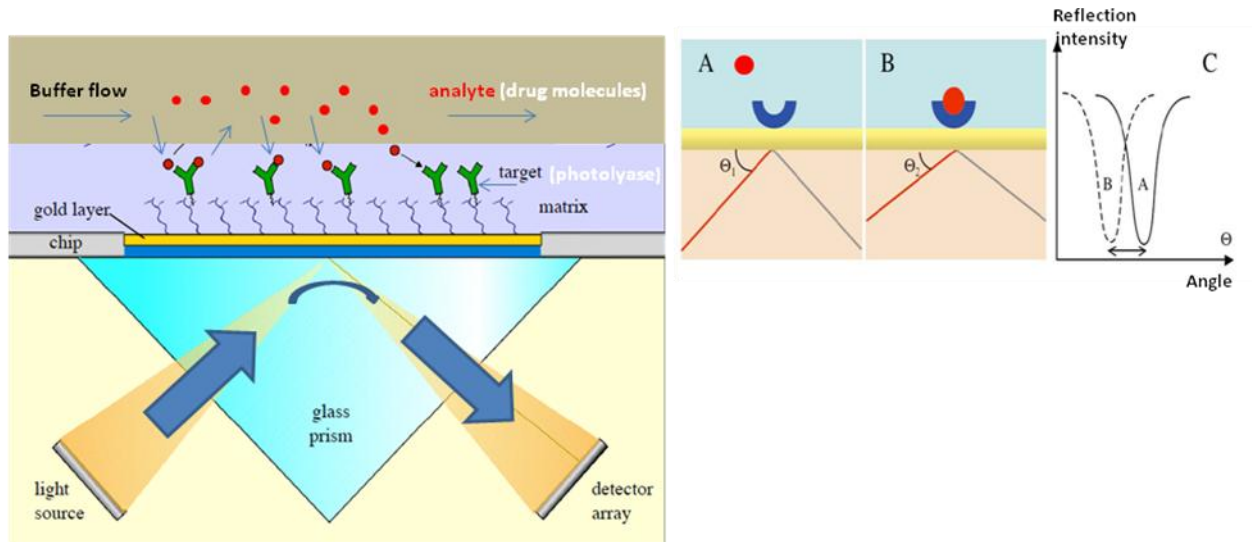
Figure 4.1 Typical SPR biosensor setup. Immobilized target molecules on the gold layer are captured by analyte molecules in injection buffer solution. This adsorption on the surface is monitored through sensor chip by detector array [55].

When the injection of analyte is stopped, the dissociation phase starts. Then the final step is the regeneration process, if needed, to remove remaining complex and reach the baseline back. Thus, SPR cycle consists of association, dissociation and regeneration phases.

4.2.3 Sensor Surface

The first step of the SPR phenomenon is the immobilization of target protein on the sensor surface. In order to analyze binding more accurately, occurrence non-specific binding should be minimized, and immobilized target should be uniformly attached to the sensor surface. Thus, various immobilization techniques have been reported for different sets of interacting biomolecules. In this study for successful SPR assays, with hydrophilic surface and diminished effects of non-specific binding, the gold surface of the sensor chip is covered with oligoethylene oxides. Oligoethylene oxides are flexible, and negatively charged molecules. Most of the

biosensors use planar sensor surface to decrease the complexity in kinetic analysis. The specifications of 2D planar SensiQ Biosensors (Nomadics Inc.) prevent artifacts and create biocompatible environment where immobilized target remain soluble. Biomolecule's direct surface attachment to gold surface may lead to loss of biological activity and uncontrollable binding. SensiQ biosensors used in this study vary for different purposes such as avidin modified gold surfaces for small reagent capture, planar carboxyl (COOH) chemistries for kinetic optimization, histidine-capture surfaces for histidine-tag ligand capture etc. Avidin modified sensor surfaces uses advantages of high affinity of biotin-avidin interaction. [62-65]

4.2.4 Equilibrium & Kinetic Measurements

Equilibrium Measurements

Equilibrium analysis helps to determine the strength of binding through two different experiment set ups. Either a several flowing analyte concentrations are injected until the signal levels out and net association equals to the dissociation [66]. Equilibrium constant, K_D, is reached when the rate of association equals to the rate of dissociation. In other words, K_D is the time required to reach the equilibrium and it could be obtained by plotting the reached response versus the analyte concentration.

$$K_D = k_d \,/\, k_a \qquad\qquad\qquad (Eq\ 4.1)$$

K_D is the equilibrium dissociation constant, which is calculated from the ratio of dissociation constant (k_d) to the association constant (k_a).

The response at equilibrium (R_{eq}) is close to the maximum response (R_{max}), which is reached as the concentration of the analyte becomes greater than K_D. While performing equilibrium analysis, it is important to use the responses of all analytes at their equilibriums [66]. K_D values lower than 10 nM are considered unsuitable for the analysis due to very slow dissociation rate and strong interactions; however, K_D values higher than 100 μM are considered comparably easy due to the weak interactions and higher dissociation rates [67].

Kinetic Measurements

SPR interactions can be fitted to different models for kinetic analysis; however, it is recommended to use the simplest model. The Langmuir model is one of the most commonly used interaction. It describes 1:1 interaction in which one ligand molecule interacts with one analyte molecule. This model adapts the pseudo-first-order kinetics and it assumes that the binding is equivalent and independent for all binding sites. The important point is that it also assumes that the reaction is not mass transport limited; contrary, it usually is [69]. Mass transport limitations are common when k_{on} values are faster than about $10^6 \, M^{-1}s^{-1}$. Given upper limit is changed with the size of the analyte. Larger molecular mass results in faster k_{on} values. This is basically due to the larger signal produced by the large analyte which allows the experiment to be performed at lower ligand densities. Consequently, lower ligand densities require lower rates of mass transport [70].

4.3 Biomolecular Interaction Model

The biomolecular interaction in the first association phase, the mobile reactant analyte (A) is flowed over the surface of the ligand (L). The concentration of the AL complex modeled in the form of pseudo-first order process. In the second dissociation phase of the complex, a buffer is allowed to flow over the surface to give free analyte and ligand. Let L be the concentration of the ligand and A be the solution concentration of the analyte. The association reaction is as in Eq 4.2:

$$L + A \quad \underset{k_d}{\overset{k_a}{\rightleftharpoons}} \quad LA \qquad \qquad (\text{Eq 4.2})$$

where k_a is the association rate constant which describes the rate of complex formation and k_d is the dissociation rate constant which describes the stability of the complex. Dissociation reaction is conversely written and given as follows:

$$LA \quad \underset{k_a}{\overset{k_d}{\rightleftharpoons}} \quad L + A \qquad \qquad (\text{Eq 4.3})$$
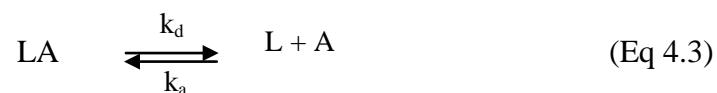
The equilibrium constant for the dissociation reaction is $K_D = k_d/k_a$. The overall rate law is derived by assuming the association reaction, Eq 4.2 and dissociation reaction, Eq 4.3 are in first order. The overall rate law is as given [71]:

$$\frac{d[AL]}{dt} = k_a[L][A] - k_d[AL] \qquad \text{(Eq 4.4)}$$

Same equation is applicable to biosensors and with the biosensor response R proportional to AL, Eq 4.5 gives:

$$\frac{dR}{dt} = k_a f_0 R_{sat} - (k_a f_0 + k_d)R \qquad \text{(Eq 4.5)}$$

where f_0 represents L, and R_{sat} represents the response at complete saturation of the immobilized binding sites.

There are several ways of analyzing the data. The simplest one is "linearization" which is putting data points in such a way to line up in a straight line. The plot gives the k_a from the slope. Usually k_d is very low and should be determined from the dissociation phase instead of the this plot. Observed rate constant is as following:

$$k_{obs} = k_a f_0 + k_d \qquad \text{(Eq 4.6)}$$

where k_{obs} represents observed rate constant. This method is found preliminary and is not used anymore. Instead, "non-linear" equations are used and integrated rate equations are obtained. This type of analysis is applied to reaction which starts without mobile reactant bound initially. The time function of binding response is given as [72,73]:

$$R(t) = R_{eq}(f_0)[1 - \exp(-k_{obs}t)] \qquad \text{(Eq 4.7)}$$

The response signal in equilibrium is given by R_{eq} as follows:

$$R_{eq}(f_0) = R_{max}[1 + \frac{k_d}{k_a f_0}]^{-1} = R_{max}[1 + \frac{K_D}{f_0}]^{-1} \qquad \text{(Eq 4.8)}$$

During dissociation phase the free mobile reactant is removed from the buffer, and for time greater than initial time R(t) is expressed as follows:

$$f_0 = 0 \text{ for } t > t_0; \quad R(t) = R(t_0)\exp[-k_d(t - t_0)] \tag{Eq 4.9}$$

4.3.1 Pros & Cons of Equilibrium Analysis

Equilibrium constants can be determined through several ways such as using the concentration of free mobile reactant or via measurement of the kinetic rate constants. The key point of using thermodynamic equilibrium approach is the independency of "mass transport" influences. Furthermore, thermodynamic equilibrium approach can be applied for those systems that are too fast for kinetic analysis. On the other hand, slow reactions and small concentrations are inappropriate for equilibrium analysis. Also, accurate determination of equilibrium can be misjudged due to the refractive index variations (buffer change) and small temperature variations or nonspecific binding. However, this problem could be solved by using multiple flow cells and comparing the signal in the absence of immobilized reactants [71,73].

4.3.2 Pros & Cons of Binding Kinetic Analysis

In data analysis part, two different strategies were proposed in order to obtain the rate constants. Those methods differ in terms of accounting the mass transport limitations. It has been pointed out that mass transport limitations and practical limitations can occur in the system. Other than that, many biomolecular interactions follow simple pseudo-first-order binding kinetics; however, there are exceptions too. In this case, the binding-process curves should be modeled with more complex rate equations. Nevertheless, binding kinetics gives "qualitative" information about complex systems as well.

4.3.3 Mass Transport Limitation

Mass transport limitation appears when the analyte association rate exceeds that rate of the analyte delivered to the surface. Upon the injection of analyte to the surface, there is association and dissociation occurs at the same time. After certain injection time, equilibrium is reached as association and dissociation rates become equal. During the dissociation phase, ideally pure dissociation is visible but in reality some rebinding of analyte can also happen. Mass transportation to the surface is enabled by both convection and diffusion. Convection of mass transport can be increased by flow rate. Rebinding is a consequence of a mass transport deficiency away from the surface. In this case, mass transport limitation can be avoided by decreasing the immobilized ligand density. Alternatively, competing molecule can be injected during the dissociation in order to block rebinding [70].

Kinetic biosensors frequently experience the limitation of binding kinetics due to the transport rate of the mobile reactant from bulk flow to the sensor surface. Accordingly, obtaining valid information about chemical kinetics becomes impossible [73]. Macromolecules may move very fast. Assuming attractive or repulsive forces are ineffective, the rate constant of an average molecule should be 10^6 $M^{-1}s^{-1}$ [74]. In other words, mass transport may affect the binding process curves with a factor of 10-100. This effect will be in both association and dissociation phase and it can be regarded as the failure of the bulk concentration f_0, the free mobile reactant at the sensor surface. In the dissociation phase, there is a positive difference between the rate of dissociation and the rate of transport. This retention effect results in a slower overall dissociation from the surface [75]. Compartment model is suggested to approximate such effects and it is given as follows [76,77]:

$$\frac{k_a^{app}}{k_a} = \frac{k_d^{app}}{k_d} = [1 + k_a(R_{sat} - R)k_{tr}]^{-1} \qquad \text{(Eq 4.10)}$$

where k_a^{app} and k_d^{app} are apparent rate constants of association and dissociation phases and k_{tr} is the phenomenological transport rate constant.

This model is highly simplified and useful in terms of describing the coupled binding and transport processes. Furthermore, it accounts for the effects of mass transport for both association and dissociation phases [78]. More accurate information can be obtained by considering the spatial distribution of the reactants. This is possible with the complex computer simulations of the reaction-diffusion process in the SPR biosensor.

In order to obtain the best results with minimum mass transport problems, it is necessary to optimize experimental conditions. The lowest binding capacity should be preferred to minimize the transport effects. As a result, high signal to noise ratio will be obtained and the data will be more reliable. In another method, different binding capacities with different surfaces can be used to prove the absence of mass transport effect [78].

4.4 SPR Experimental Setup

In this thesis, SPR analysis was performed on a SensiQ Discovery (ICX Nomadics, Oklahama City, OK, USA) system using neutravidin modified sensor chips (BioCap Chip, SensiQ Discovery). BioCap Chip is prepared from a planar carboxylated surface by immobilizing neutravidin on the surface by amine coupling.

SensiQ Discovery is a dual channel SPR based instrument which has two injection ports and loops. Each injection loop is loaded with a standard sample loading syringe. The flow rate is controlled from control interface of SensiQ software. The user is prompted by the software to turn the injection valve inject/load position in the beginning and end of the injection process. In general, one of the channels is used as a reference, while the other has immobilized ligand. Technical specifications of SensiQ Discovery are given in Appendix A5.

All SPR results were acquired using the instrument software SensiQ Discovery (version B.00, build 2.0.0). Data processing for kinetic analysis were performed in Qdat Data Analysis Tool (version 1.0.0.24; Nomadics Inc.)

4.4.1 SPR Reagents

In SPR experiments, running buffer was prepared from 1X PBS tablet (purchased from Sigma Aldrich) in 200 mL dH$_2$O (10 mM phosphate buffer, 2.7 mM KCl, 137 mM NaCl, 100 mM Na$_2$HPO$_4$, 1.76 mM KH$_2$PO$_4$, pH 7.4). 0.005 % Tween20 was also added into the running buffers as surfactant to prevent the non-specific protein binding to sensor surface. Immobilization and injection buffers were also prepared from 1X PBS buffer. Sodium dodecyl sulphate (SDS, 0.1 %) was used as regeneration and instrument cleaning buffer in order to remove non-specific bindings due to hydrophobic interaction. All other reagents were purchased from Sigma Aldrich. All buffer solutions were degassed using a vacuum pump. Buffer pH values were checked with a pH-meter (PHM 210, MeterLab) equipped with a combined pH glass electrode.

4.4.2 Preparation of Target Protein and Drugs

E.coli DNA photolyase was chosen as the target protein in this study. Since neutravidin modified gold surface, BioCap Chip was used as sensor surface, DNA photolyase was biotinylated as described in Chapter 3.

In this thesis, out of 2400 compounds of computational studies, eight were chosen to be investigated with SPR due to their commercial availability. It should be noted that these compounds were not purchased in the pure form, but there are active ingredients of these commercial drugs. Lornoxicam was the only pure compound available in this study (supported by producer company, Abdi Ibrahim A.Ş., Turkey), others were in the form of commercial drugs with inactive ingredients. All eight drugs were purchased from local pharmacy store in Sarıyer, Istanbul. Compounds, inactive ingredients and their brand names are given in Table 4.2.

Table 4.2 Commercial name of drugs used for SPR experiments

Active Ingredient	Commercial Name
Prednisone	Deltacortril
Triamcinolone	Sinakort A
Fenofibrate	Lipanthyl 267
Clomifene	Serophene 50
Lornoxicam	Xeforapid
Azelastine	Allergodil Nazal Sprey
Desloratadine	Deloday
Rupatadine	Rupafin

Drugs in Table 4.2 were dissolved and made ready to be used in experiments with the following procedure: first, a calculated amount of drug were dissolved in 100 % DMSO solution and added to SPR running buffer (pH 7.4) as the concentration of compound become 1 mM (with 0.3% DMSO). Then, drug solutions were serially diluted again with SPR running buffer (pH 7.4); drug concentrations of 100 µM, 10 µM, 1 µM with very dilute DMSO concentrations, of 0.03 %, 0.003 %, and 0.0003 %, respectively.

In order to avoid specific binding of molecules other than the analyte and eliminate bulk solvent shifts, all buffers were filtered before use. By doing so, filter frits which are positioned at the injection ports were kept clean. Furthermore, buffers were degassed everyday either by keeping them under vacuum or treating them in ultrasonic bath for at least 15 minutes. The very common procedure for running buffer preparation consists of filtering all buffers which are larger in volume than 100 mL. For this procedure 0.45 µm filters were used and vacuuming was preferred for degassing. Samples between 3 mL-100 mL was filtered with the same filters; however, degassed with ultrasonicator. Finally, samples with a volume lower than 3 mL was centrifuged with 5000 Hz for 5-10 minutes and then degassed by vacuuming. All the buffer samples were centrifuged for a few seconds to avoid formed air bubbles. All vials closed tightly to prevent evaporation.

4.4.3 Instrument Maintenance

The manufacturer supplies information about the maintenance of the device and in order to have long time instrument life and sufficient, correct data collection, manual should be followed accordingly. Every week and before every new experiment set, the system should be cleaned thoroughly. For this process 0.1% SDS was used and it was followed by 100 nM NaOH with a pH of 13. Cleaning increases the data quality. It is recommended not to turn the system off, but keeping the constant flow of assays. Each new assay was injected after cleaning the system with 0.1 % SDS followed by distilled water. Before injection, the port is cleaned with air followed by distilled water. This procedure is repeated at least five times to make sure that system was free of buffer. In addition, needles and syringes were cleaned on a regular daily basis.

4.4.4 Initial preparation of new sensor chips

In order to minimize the impurity effect, each sensor chip was treated with the regeneration solution before use. If it is not possible to clean the sensor chip, it is recommended to use a new chip. After insertion, SPR dip signals were checked in order to be sure that the normalization of the refractive index is sufficient and SPR dip is successfully established (Figure 4.2). An air bubble may change the dip signal of SPR due to the sudden change of binding signal. Main reason for that is the refractive index of the air is much lower than the refractive index of the buffer used. Such a big change in the refractive index values will result in a sharp drop in the response signal. Therefore, the system should be free of air before use. PBS buffer with a pH of 7.4-7.5 should run at least three times. The response versus time data should be collected via SensiQ Discovery program for at least 60 minutes, so a stable baseline for the response could form.
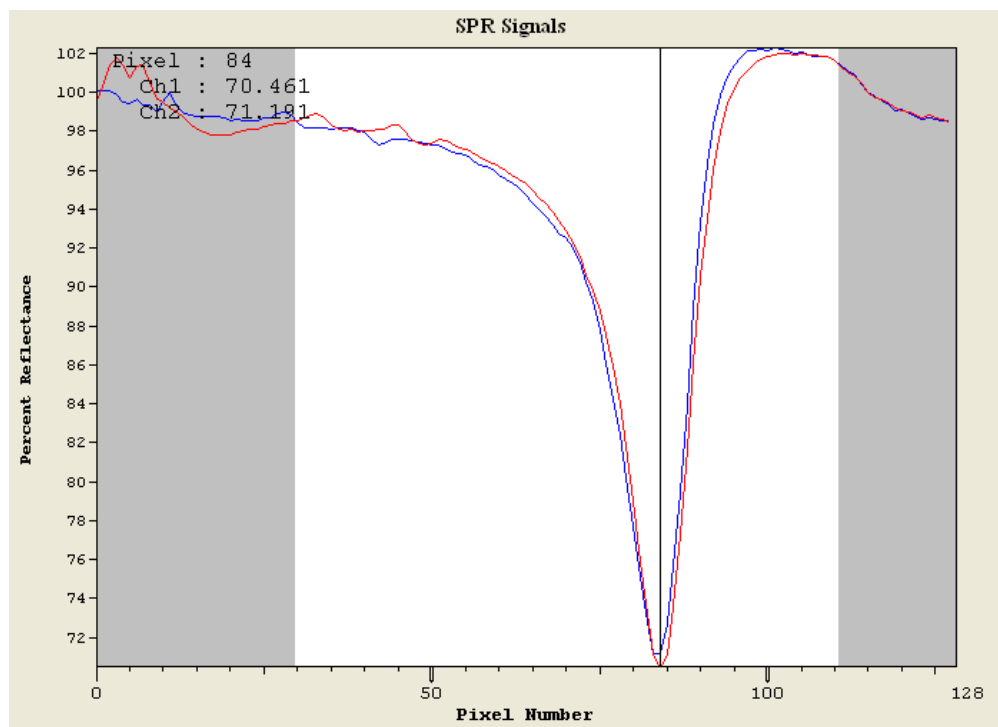
Figure 4.2 SPR dips for both channels were established in almost same pixel number and percent reflectance. Red represents Channel 1, whereas blue represents Channel 2.

4.5 SPR Results and Discussion

This part of the study focuses on experimental investigation of DNA photolyase/drug interaction via SPR and comparison of results with computational model. Most common method for this comparison is based on equilibrium dissociation constant, K_D. Although there is no theoretical limitation on comparing K_D values from AutoDock and SPR, the validity of this comparison was the question. However, in the literature, there exist various protein/small molecule interaction studies showing very good correlations between K_D values from both AutoDock and SPR [79-81]. In one study, Li et al. investigated binding of drug-like molecules on Human 5-Lipoxygenase (5-LOX) protein by both AutoDock and SPR. Results showed that AutoDock-predicted binding free energies for the drug-like molecules showed a good correlation between the K_D values measured by SPR assay and the experimental values in the literature which is represented as IC_{50} (the half maximal inhibitory concentration) value [81].

As discussed before, commercial drugs were investigated in SPR experiments (see Appendix A6 for detailed information about these drugs). These commercial drugs consist of target compound as an active ingredient as well as inactive ingredients (excipients) as a part of these drugs. Most of drugs do not include information about excipients for commercial reasons; only mass ratio of active ingredient within the drug capsule was provided. The phenomenon which deals with drug binding analysis with inactive drug ingredients on target protein via SPR has not been studied yet. Our assumption for this phenomenon was that since inactive drug ingredients are not designed to specifically interact with target protein, it was supposed to have ignorable effects in SPR assays as these inactive ingredients would not compete with active ingredients in terms of specific binding. The effect of presence of inactive ingredients to drug-protein interaction has only been investigated with lornoxicam, due to its availability, and negligible differences have been obtained in SPR responses between the pure lornoxicam and the same drug as in the form of commercial pill. In the literature, there is no study concerning SPR binding analysis with commercial form of drugs. Hence, the results obtained in this study can lead to important improvements in early stages of drug discovery, as large number of compounds could be screened via SPR without the need to label or purify active drug candidates.

4.5.1 SPR Assay

Experimental parameters have been optimized to eliminate non-specific binding and mass transport limitations in SPR experiments. Non-specific binding was minimized after certain amount of Tween 20 was added to running buffer as 1x PBS buffer with 0.005% Tween 20. In order to diminish mass transport limitations, amount of immobilized protein was optimally minimized whereas concentration of drug was kept high. Thus, only 150-250 RU of protein was immobilized. Optimized condition for drug samples were as follows: 3 drug concentrations, 10-fold each, were prepared as 100 μM, 10 μM, 1 μM with very dilute DMSO concentrations of 0.03%, 0.003%, and 0.0003%, respectively. Thus, the need for DMSO calibration was omitted. In each injection, 50 μl of drug sample was injected with a flow rate of 50 μl/min to both reference and target channel. In this assay condition, less than 1 μM of drug concentrations led to mass transport limitations, observed as irrelevant increases in response units due to continuous

rebinding of drug molecules. Therefore, drug concentrations were optimized as 1-100 µM. However, 100 µM drug concentration was excessive amount for some drugs and showed non-specific accumulations on the surface rather than binding, thus these unreliable data was also omitted. In general, no regeneration buffer was used; regeneration was done by natural dissociation until reaching baseline back. Thus, adequate amount of time was given between each injection (1-2 hours). If needed, 0.1% SDS buffer was applied as regeneration buffer.

As mentioned earlier, data analysis method is determined as kinetic data analysis according to the some parameters discussed before; such as mass transport limitation, interaction speed, ligand and analyte size, time consumed etc [71].

During kinetic parameter analysis in Qdat, some important criteria were applied. First, all data were blanked and referenced. Next, residual standard deviation (ResSD), the measure for the goodness of model fit as the average difference between simulated curve and experimental curve was kept in the range of 5-10% of maximum response reached in the data, as suggested by Qdat tutorial. Qdat analysis tool can also estimate quantitatively via mass transport limitation calculator (% MTL). Qdat tutorial suggests that if % MTL is less than %5, no significant mass transport limitation is observed. For each drug set % MTL was checked as below 5%, then simple k_a and k_d model was used [82]. SPR experiments started with immobilization of DNA photolyase on BioCap Chip sensor surface. Next, nine sets of drugs (eight commercial, one pure lornoxicam) were injected onto the surface. Finally, K_D values for nine sets of drugs (see Table 4.2) were calculated via Qdat using pseudo-first order interaction model.

4.5.1.1 Immobilization of DNA photolyase

Due to its simplicity, avidin-biotin based immobilization method was preferred, thus neutravidin modified BioCap Chip was used as a sensor surface. BioCap surface is prepared by immobilizing neutravidin onto a planar surface containing carboxyl groups by amine coupling. Neutravidin was chosen since it exhibits very low non-specific binding. It is reported that

biotinylated ligand was immobilized on neutravidin surface with extremely high affinity, typically around 10^{-12} M [82].

During immobilization step, 10 nM-100 nM of biotinylated DNA photolyase was injected in first channel while blank running buffer was injected in second one as reference channel. The difference between the response after dissociation phase and the response before association shows the amount of the conjugate immobilized tightly on the sensor surface.
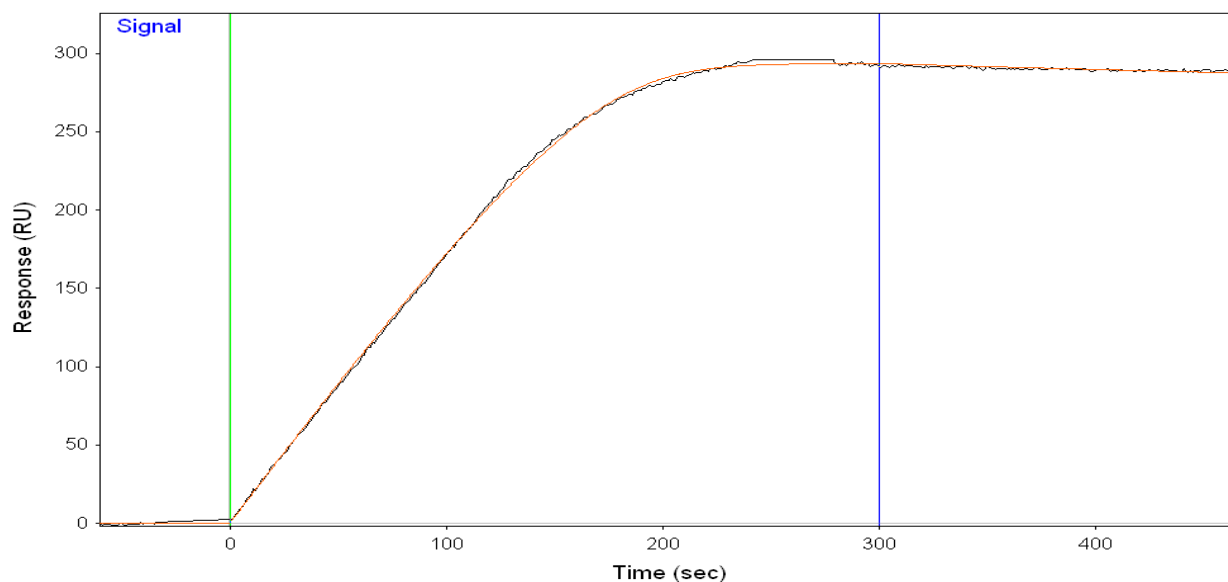
Figure 4.3 Injection of biotinylated DNA photolyase (10nM) on BioCap Chip. Red (model fit), green (injection start), blue (injection end) (20 µl/min flow rate, 100µl injection volume).

Table 4.5.1.1 Binding analysis of biotinylated photolyase on neutravidin modified surface

k_a (M^{-1}s^{-1})	k_d (s^{-1})	K_D (pM)
8.17e6	1.40e-4	**17.20**

In Figure 4.3, referenced and blanked data has shown that immobilization of DNA photolyase was successfully done. After injection end, slow dissociation rate represents high binding affinity. Kinetic parameters for this binding were analyzed by using model fit via Qdat. The equilibrium dissociation constant, K_D, was calculated as, 17.20 pM. (Table 4.5.1) This value is less than measured dissociation constants of biotin-avidin interaction, $K_D \approx 10^{-15}$ M due to

steric hindrance effect but is similar to the K_D value ($K_D \approx 10^{-12}$) measured for neutravidin-biotin surface. [82, 83].

4.5.1.2 DNA photolyase vs Lornoxicam (pure)

Lornoxicam is a nonsteroidal drug used as anti-inflammatory drug from oxicam family. It is effective to relieve analgesic (pain reliever) and antipyretic (fever reducer) symptoms. However, it differs from the oxicam family with its potential of inhibiting the prostaglandin biosynthesis and its particular efficacy is explained with this difference. Molecular weight of Lornoxicam is 371.81 g/mol. Lornoxicam has 3-4 hours biological half-life which represents the time for a drug to lose half of its pharmacologic activity [84].

Predicted K_D value for Lornoxicam (Lor) with AutoDock was 8.52 µM. In Figure 4.4, pure form of Lornoxicam was injected onto immobilized DNA photolyase with three different concentrations as mentioned before and injections were repeated three times in order to ensure more reliable data fitting. Lornoxicam concentration of 100µM was omitted, as high drift in SPR responses resulted in accumulation rather than binding. Results show that K_D values calculated via Qdat was found out less than AutoDock predictions, but order of magnitude was still similar (See Table 4.5.1.2).
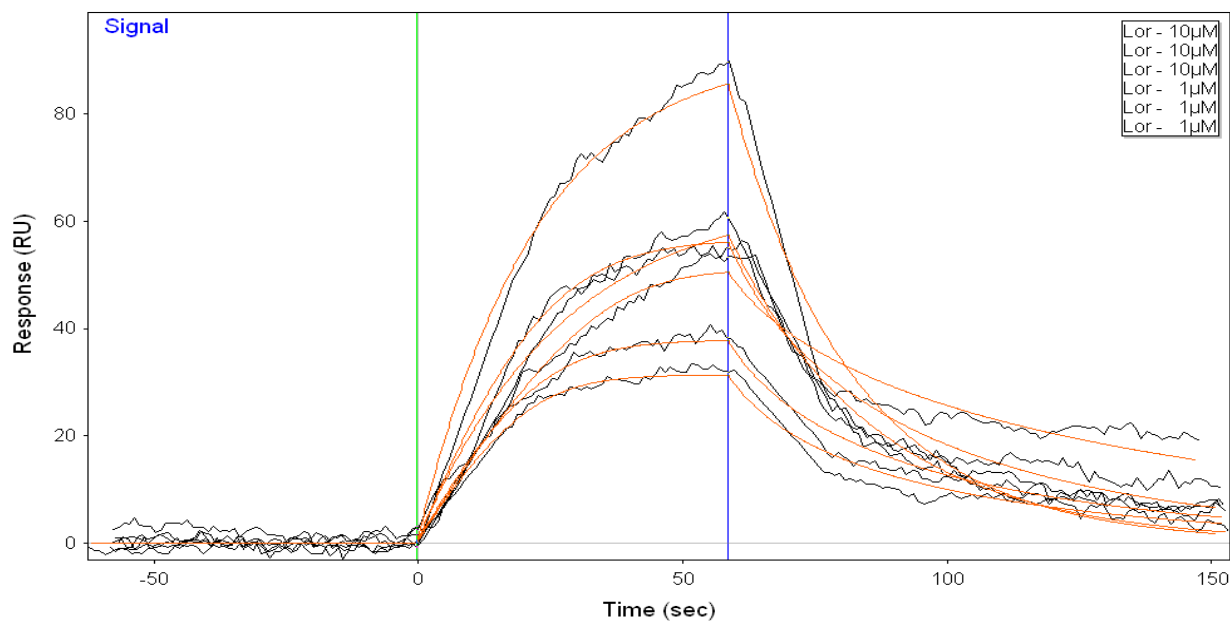
Figure 4.4 Lornoxicam (pure) (50μl/min flow rate, 50μl injection volume).

Table 4.5.1.2 Kinetic binding parameters of Lornoxicam on immobilized DNA photolyase

k_a (M^{-1}s^{-1})	k_d (s^{-1})	K_D (μM)
6214.3	0.024	**3.94**
6647.7	0.024	**3.71**
6889.9	0.017	**2.55**
4463.8	0.012	**2.77**
6576.1	0.024	**3.66**
8830.8	0.019	**2.19**

4.5.1.3 DNA photolyase vs Lornoxicam

Next compound was commercial drug form of Lornoxicam. Figure 4.5 shows response curves for Lornoxicam injections in the form of a commercial. In order to get more reliable data set, some parameters were re-optimized; these experiments were performed using 1x PBS without Tween 20 and longer injection times. Therefore, higher RU was obtained in Figure 4.5. Since K_D is the ratio of association constant (k_a) to dissociation constant (k_d), the high or less RU

is not the sole indicator in explaining binding event. Finally, equilibrium dissociation constant, K_D values were calculated and tabulated in Table 4.5.1.3. This set of SPR assay showed that calculated K_D values for commercial Lornoxicam were similar to the values obtained for pure Lornoxicam. Slight differences obtained between the pure and commercial drug lornoxicam could be attributed to the steric effect caused by the inactive ingredients present in the commercial drug. Also, it should be noted that approximately ten fold decrease in both k_a and k_d were obtained when comparing to these values with values for pure Lornoxicam. This means slower association and dissociation rates have been obtained for commercial drug compared to the rates measured for pure lornoxicam. This can also be explained by possible non-specific binding due to the differences in the running buffer. Tween 20 surfactant which minimizes the non-specific binding events was used for the experiments with pure lornoxicam, while in the experiments with commercial lornoxicam this surfactant was not used.

In conclusion, results of binding kinetics from both pure and commercial form of Lornoxicam have shown very good correlation with computational model in terms of binding constants. Also, our assumption, which claims inactive ingredients show no significant effect in terms of K_D values, was preliminarily validated with Lornoxicam, but still needs to be confirmed for other drugs when pure compounds are available.
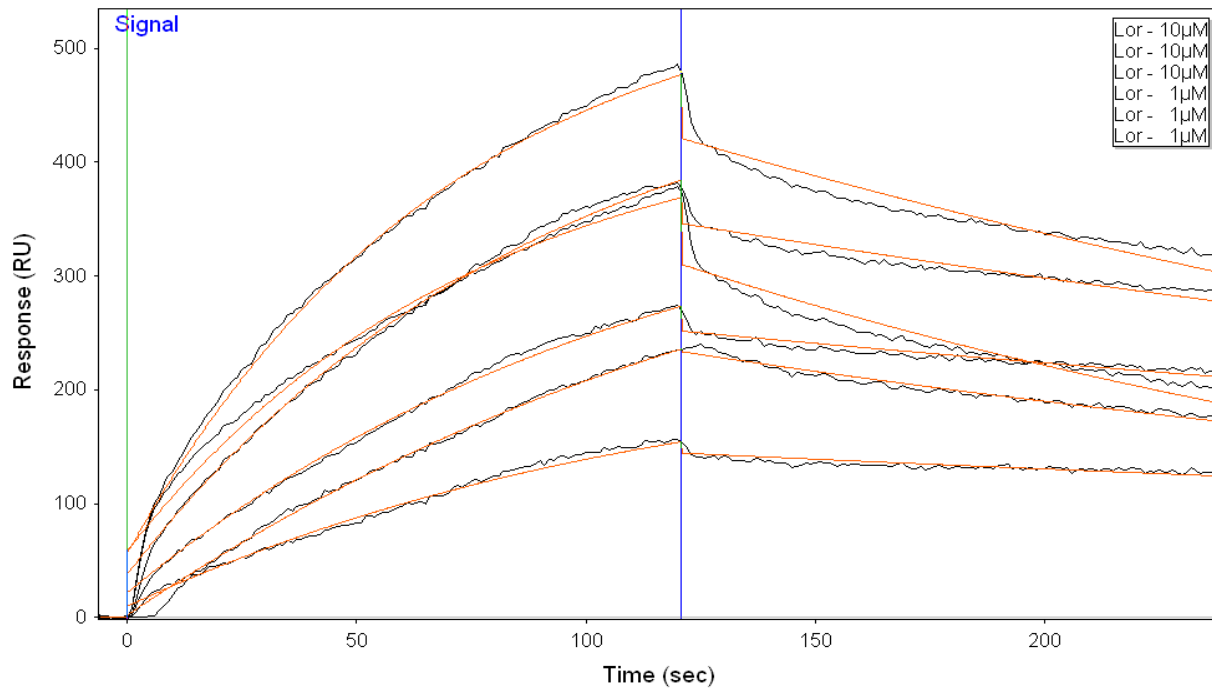
Figure 4.5 Lornoxicam (commercial) **(**50µl/min flow rate, 100µl injection volume)

Table 4.5.1.3 Kinetic binding parameters of Lornoxicam on immobilized DNA photolyase.

k_a $(M^{-1}s^{-1})$	k_d (s^{-1})	K_D (μM)
572.0	1.56e-3	**2.73**
582.8	1.76e-3	**3.02**
631.9	2.19e-3	**3.47**
683.3	2.14e-3	**3.13**
726.6	3.56e-3	**4.90**
639.4	4.58e-3	**7.17**

4.5.1.4 DNA photolyase vs Fenofibrate

Fenofibrate is a drug used to reduce the cholesterol levels in patients at risk of cardiovascular disease. It's from the fibrate class and like other fibrates it reduces both low density lipoprotein (LDL) and very low density lipoprotein (VLDL) levels. On the other hand, it

increases high density lipoprotein metabolic syndrome. Its molecular weight is 360.83 g/mol. Its half life is 20 hours [84].

Predicted K_D value for Fenofibrate by AutoDock was 30.58 µM. Table 4.5.1.4 gives the results of calculated SPR K_D, in range of 14.4 – 45.6 µM which has a good correlation with computational model.
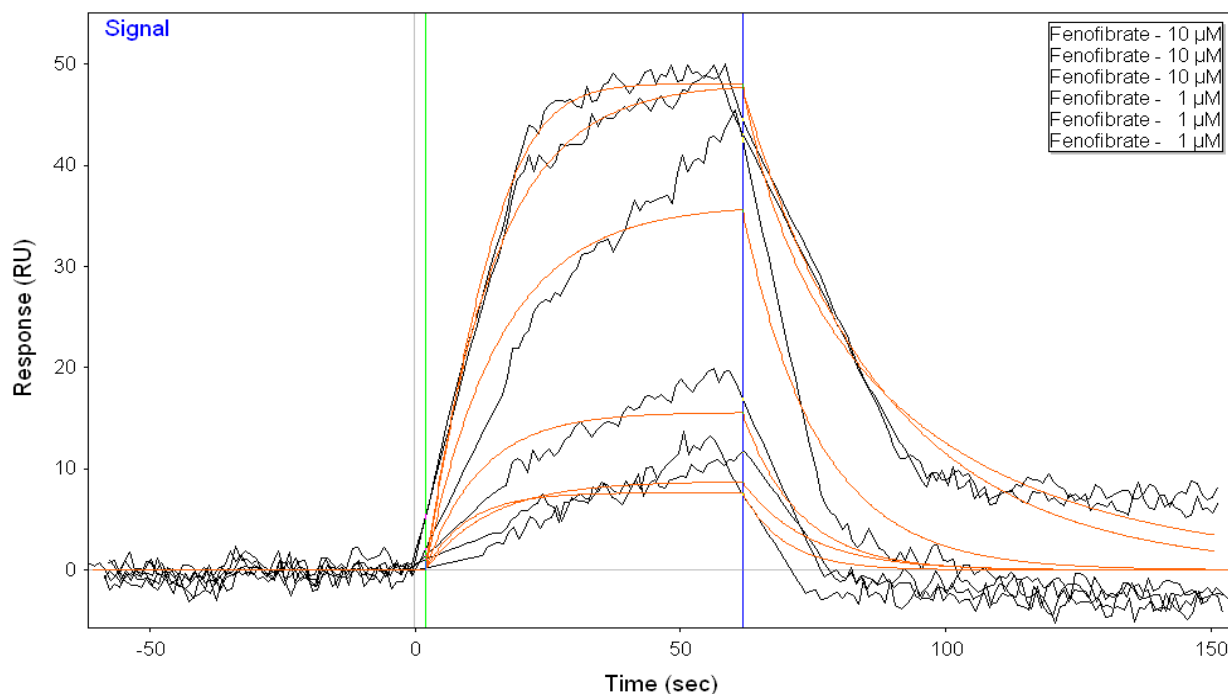
Figure 4.6 Fenofibrate (commercial) (50µl/min flow rate, 50µl injection volume)

Table 4.5.1.4 Kinetic binding parameters of Fenofibrate

k_a (M^{-1}s^{-1})	k_d (s^{-1})	K_D (µM)
2741.5	0.125	**45.62**
2508.1	0.080	**32.29**
3577.8	0.092	**25.93**
4582.6	0.065	**14.40**
1960.6	0.041	**21.11**
2207.9	0.045	**20.66**

4.5.1.5 DNA photolyase vs Clomifene

Clomifene is a triphenyl ethylene stillbene derivative. It is a selective estrogen receptor modulator. It increases the production of gonadotropins by inhibiting the negative feedback on the hypothalamus. It is used for the treatment of female infertility [84].

Predicted K_D value for Clomifene by AutoDock was 43.23 µM. Table 4.5.1.5 gives results of calculated SPR K_D, in range of 25.18 – 90.02 µM.
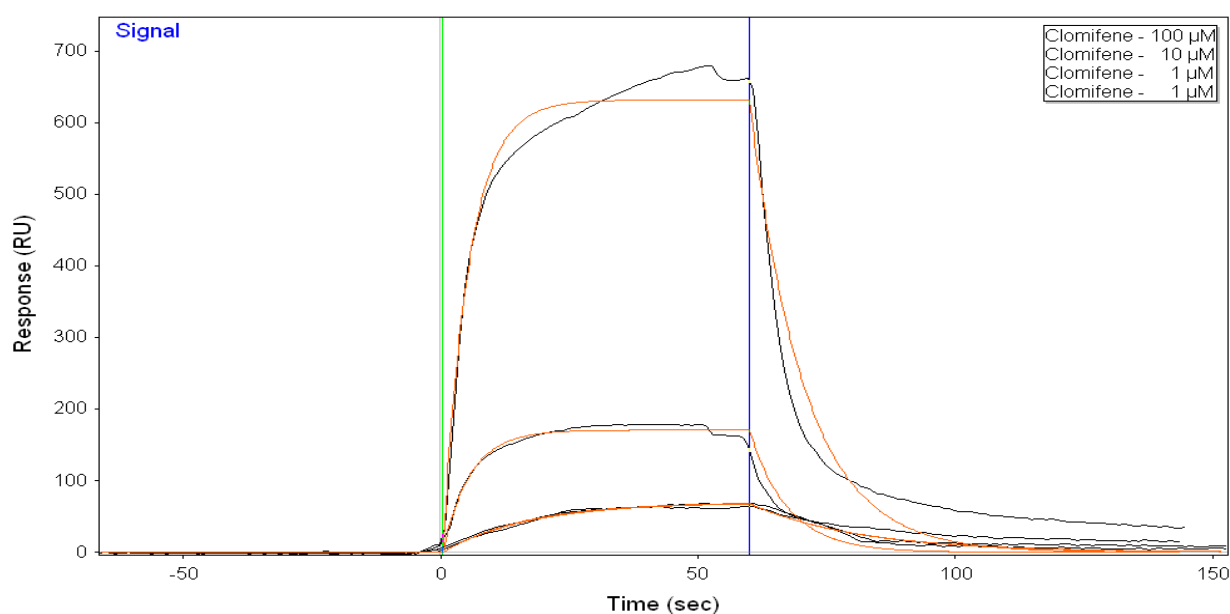
Figure 4.7 Clomifene (commercial) (50µl/min flow rate, 50µl injection volume)

Table 4.5.1.5 Kinetic binding parameters of Clomifene

k_a ($M^{-1}s^{-1}$)	k_d (s^{-1})	K_D (µM)
1048.1	0.094	**90.02**
5349.5	0.134	**25.18**
1384.9	0.045	**33.19**
1433.5	0.047	**32.85**

4.5.1.6 DNA photolyase vs Prednisone

Prednisone is a synthetic anti-inflammatory drug and a derivative of corticosteroids. Its main effectiveness occurs as an immunosuppressant. In addition, it is also used in treatment of cancer. Although it is synthetic, this drug is biologically inert and it is converted to prednisolone in the liver. Its molecular weight is 358.4281 g/mol, half life is 1 hour [84].

Predicted K_D value for Prednisone (Pred) by AutoDock was 316 nM. Table 4.5.1.6 gives results of calculated SPR K_D, in range of 398 nM – 20.51 µM.
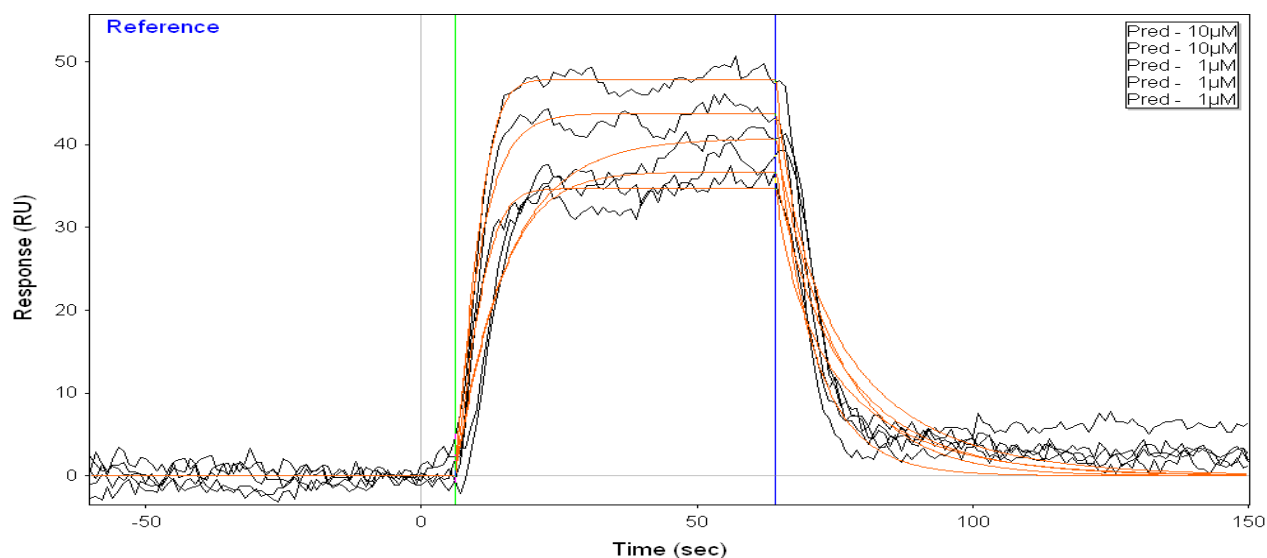
Figure 4.8 50µl/min injection of 50µl of Prednisone (commercial)

Table 4.5.1.6 Kinetic binding parameters of Prednisone

k_a $(M^{-1}s^{-1})$	k_d (s^{-1})	K_D (µM)
57149.5	0.060	**1.05**
91386.6	0.093	**1.02**
2.184e5	0.091	**0.41**
1.212e5	0.048	**0.39**
27732.8	0.081	**2.92**

4.5.1.7 DNA photolyase vs Azelastine

Azelastine is a second generation antihistamine which is a derivative of phthalazine. Just manipulating the volume ratio, azelastine can be used both as a nasal spray and as an eye drop. Azelastine has molecular weight of 381.89 g/mol and half life of 22 hours [84].

Predicted K_D value for Azelastine (Aze) by AutoDock was 687 nM. Table 4.5.1.7 gives results of calculated SPR K_D, in range of 924 nM – 16.01 µM.
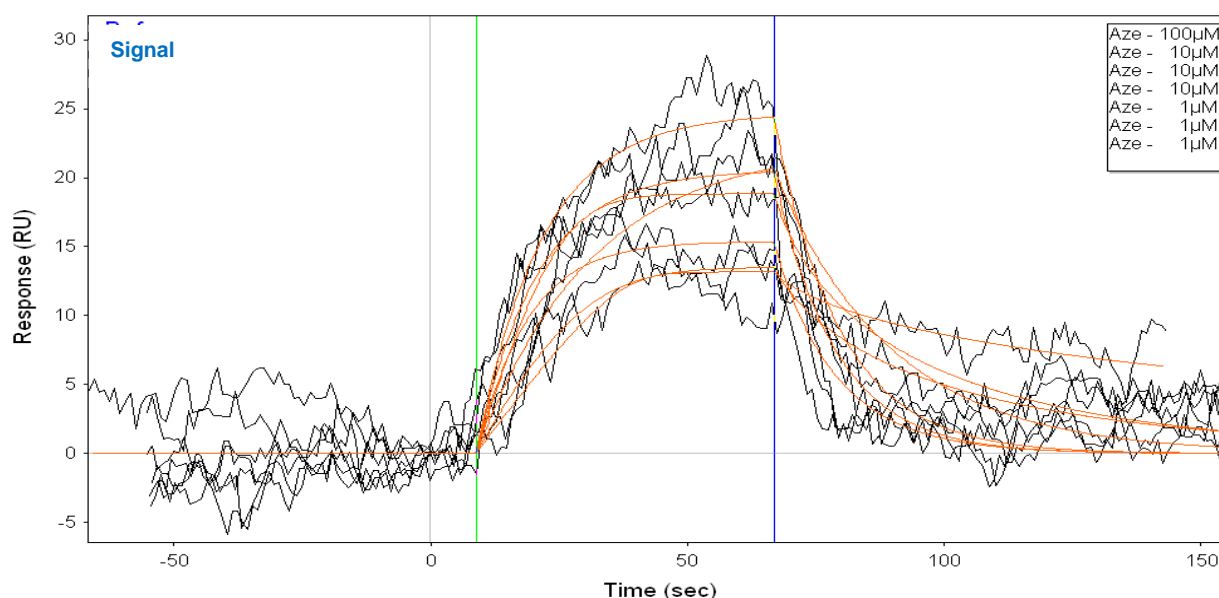
Figure 4.9 Azelastine (commercial) (50µl/min flow rate, 50µl injection volume)

Table 4.5.1.7 Kinetic binding parameters of Azelastine

k_a ($M^{-1}s^{-1}$)	k_d (s^{-1})	K_D (µM)
52285.0	0.066	**1.27**
49848.6	0.084	**1.68**
85833.4	0.079	**0.92**
2615.5	0.041	**16.01**
3321.7	0.040	**12.16**
3559.9	0.038	**10.91**
622.7	7.835e-3	**12.58**

4.5.1.8 DNA photolyase vs Desloratadine

Desloratadine is used for treating allergies and it is a tricyclic antihistamine. It is second generation histamine. Its effect lasts long and does not cause drowsiness because it takes some time to go into the central nervous system. Desloratadine has molecular weight of 310.82 g/mol and half life of 27 hours [84].

Predicted K_D value for Desloratadine (Des) by AutoDock was 426 nM. Table 4.5.1.8 gives results of calculated SPR K_D, in range of 657 nM – 3.45 µM.
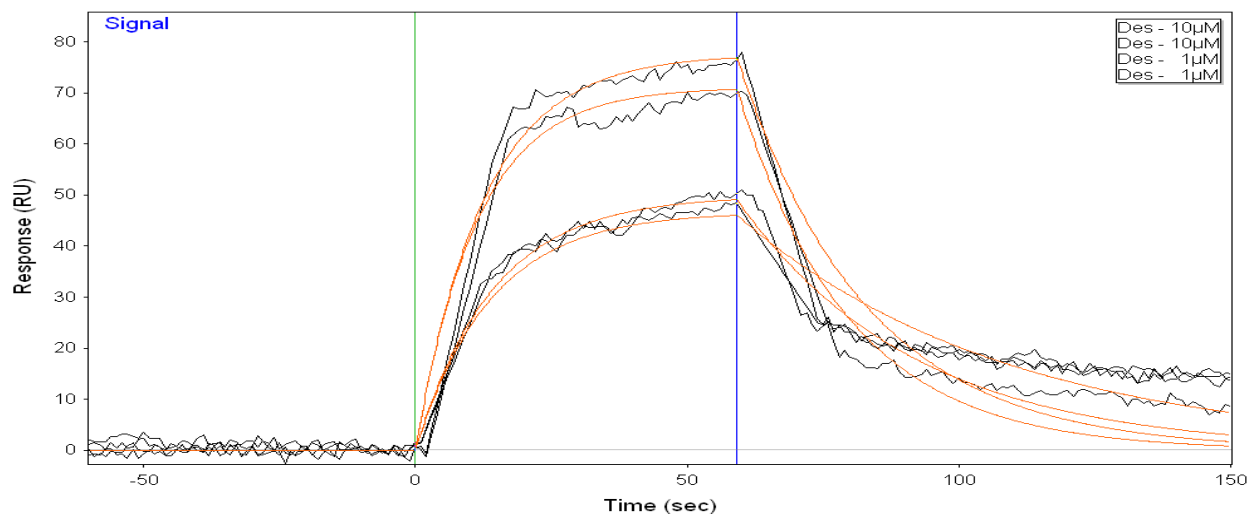
Figure 4.10 Desloratadine (commercial) (50µl/min flow rate, 50µl injection volume)

Table 4.5.1.8 Kinetic binding parameters of Desloratadine

$k_a\ (M^{-1}s^{-1})$	$k_d\ (s^{-1})$	$K_D\ (µM)$
57838.8	0.038	**0.65**
12181.2	0.110	**0.90**
24767.4	0.034	**1.38**
33914.5	0.117	**3.45**

4.5.1.9 DNA photolyase vs Rupatadine

Rupatadine is a second generation antihistamine and PAF antagonist which is used to treat allergies. Rupatadine has molecular weight of 415.96 g/mol and half life of 6 hours [84].

Predicted K_D value for Rupatadine by AutoDock was 1.08 µM. Table 4.5.1.9 gives results of calculated SPR K_D, in range of 1.23 – 11.77 µM.
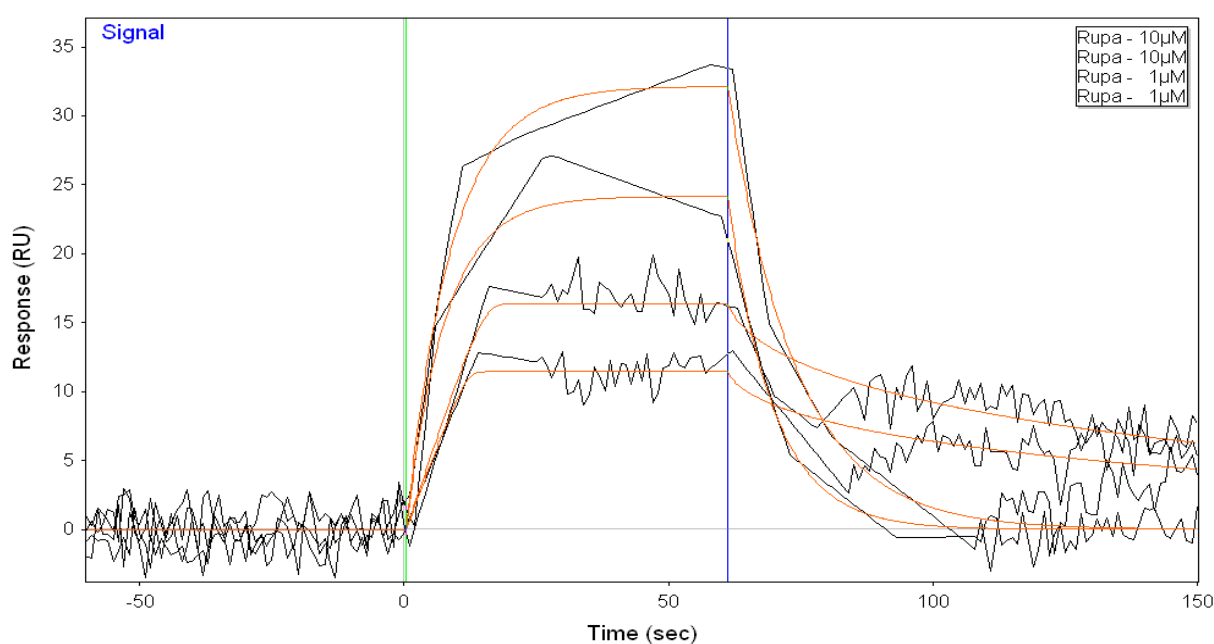
Figure 4.11 Rupatadine (commercial) (50µl/min flow rate, 50µl injection volume)

Table 4.5.1.9 Kinetic binding parameters of Rupatadine

k_a (M⁻¹s⁻¹)	k_d (s⁻¹)	K_D (µM)
23019.4	0.031	**1.38**
38222.3	0.047	**1.23**
7374.0	0.067	**9.21**
7649.0	0.090	**11.77**

4.5.1.10 DNA photolyase vs Triamcinolone

Triamcinolone is a synthetic corticosteroid and it has a long lasting effect. Since it is free of alcohol or esterified forms, it can be taken orally, intramuscularly, by injection or as a topical ointment. Triamcinolone has molecular weight of 394.43 g/mol and half life of 88 minutes [84].

Predicted K_D value for Triamcinolone by AutoDock was 982 nM. Table 4.5.1.10 gives results of calculated SPR K_D, in range of $2.20 - 31.12$ µM.
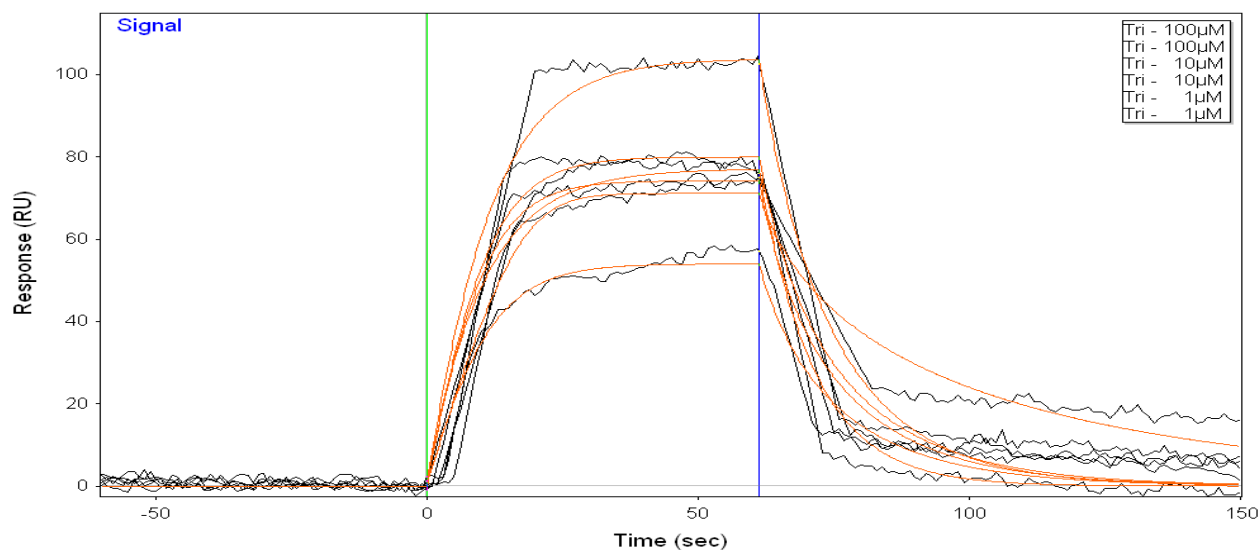
Figure 4.12 Triamcinolone (commercial) **(**50µl/min flow rate, 50µl injection volume)

Table 4.5.1.10 Kinetic binding parameters of Triamcinolone

k_a ($M^{-1}s^{-1}$)	k_d (s^{-1})	K_D (µM)
43120.8	0.095	**2.20**
15882.6	0.035	**2.24**
7661.9	0.098	**12.79**
7061.9	0.219	**31.12**
4743.1	0.080	**16.97**
7784.4	0.114	**14.66**

4.5.1.11 MBP vs All Drugs

Since DNA photolyase was purified with maltose binding protein (MBP), biotin-photolyase conjugathas also MBP. Therefore, the interaction of MBP with all drugs should have also been analyzed (Figure 4.13). MBP was biotinylated using the same protocol used for photolyase biotinylation, and immobilized on neutravidin functionalized Biocap surface (150-250 RU). Next, all drugs with a concentration of 10 µM were injected onto both channels.

Results show that none of the drugs specifically bind to MBP, since referenced data gathered with subtraction of reference channel, in which neutravidin was immobilized as a part of BioCap Chip was almost zero or negative. This shows that drugs bind to MBP with affinity similar toneutravidin, therefore, the presence of MBP in photolyase structure did not affect binding analysis.
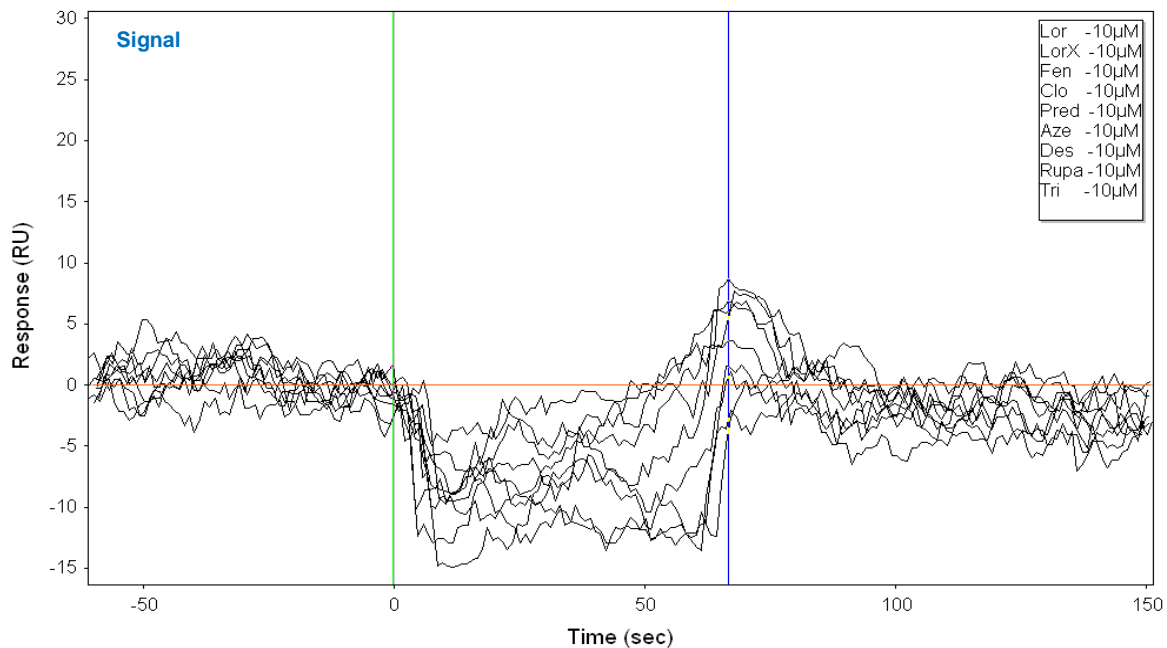
Figure 4.13 Injection of drugs on MBP

(LorX represents pure form of Lornoxicam) (50µl/min flow rate, 50µl injection volume).

4.6 Overall of SPR Results

The objective of this part was experimental validation of K_D values predicted by computational model in photolyase/drug interaction. In Table 4.6.1, all SPR results are summarized and compared with AutoDock predictions. SPR results have shown very good correlation with AutoDock predictions in terms of binding constant, K_D. As was predicted by AutoDock, K_D values of protein/drug interactions are quite close to each other. In SPR experiments, there are some variations in K_D values, especially for different concentrations of the same drug. Mzyska et al. claims that analyte concentration for an ideal SPR assay should have same order of magnitude with K_D and it is convenient to vary concentration of analyte in the range of 0.1-100 times K_D in order to obtain accurate binding constant of interaction [71]. In this study, analyte concentrations for SPR assays were also kept within the suggested range of 1-100 µM.

Table 4.6.1 Comparison of AutoDock and SPR Results

Drugs	AutoDock K_D (µM)	SPR K_D (µM)
A07EA03 - Prednisone	0.31	0.39 - 2.92
R06AX27 - Desloratadine	0.42	0.65 - 3.45
R06AX19 - Azelastine	0.68	0.92 - 16.01
A01AC01 - Triamcinolone	0.98	2.20 - 31.12
R06AX28 - Rupatadine	1.08	1.23 - 11.77
M01AC05 - Lornoxicam	8.52	2.19 - 7.17
C10AB05 - Fenofibrate	30.58	14.40 - 45.62
G03GB02 - Clomifene	43.23	25.18 - 90.02

Although, kinetic constants of binding from results of AutoDock and SPR are compared in this study, one important point should be noted; with AutoDock, we analyzed site specific binding (drug binding to FAD region of DNA photolyase), however SPR analysis does not give any information about where the analyte is specifically bound. Our approach to make more reliable kinetic analysis in terms of specificity of binding was based on eliminating the non-specific portion of the binding in the SPR kinetic analysis. Van der Merwe et al. claims that the amount of non-specific binding over total binding could be approximated by immobilizing a reference protein to the reference channel, where protein size needs to be similar to the target protein and that the reference protein has no binding affinity to the corresponding drug compounds [77]. In the literature, the most common protein used for this purpose is bovine serum albumin (BSA). Basic methodology is to obtain BSA/drug interaction which is considered as non-specific interaction and deduct it from the target protein/drug interaction. But in this study, there is no need to immobilize BSA to the reference channel for this purpose, as BioCap Chip surface has already immobilized protein, neutravidin whose molecular mass is approximately 60 kDa whereas BSA is 66kDa, and it was observed that drugs show no specific interaction with neutravidin. In summary, portion of the non-specific binding was minimized with neutravidin based approach to obtain more reliable kinetic data parameters.

As a conclusion of this part, main findings could be summarized as follows:

●   For the first time in the literature, the binding interactions of DNA photolyase with small molecules were directly measured and real time analysis of kinetic parameters was performed via SPR.

●   Prednisone, Desloratadine, Azelastine were found to have highest binding affinity ($K_D \approx$ 0.39 - 3.02μM, 0.65 - 3.4μM, 0.92 - 16.01μM, respectively)) to the DNA photolyase. This is an early stage of drug discovery, these drugs can be modified and optimized to increase specificity of binding, and then can be validated through further biological inhibition assays.

- No significant differences between pure Lornoxicam compound and commercial form of Lornoxicam drug (with inactive ingredients) binding to DNA photolyase has been found in terms of kinetic binding constant.

- SPR results are found to be in good agreement with computational model prediction, in terms of K_D values from both AutoDock and SPR.

4.7 Remarks

Since this study focuses on FDA approved drugs, outcome of this study can reveal new side effects of these drugs or interpret existing side effects at the molecular level. In Appendix A6, detailed information for all 8 drugs used in SPR experiments was given as description, side effects and properties of these drugs. There is an interesting point in Appendix A6 from side effects of Prednisone. Lozado et al. showed that insomnia is the chief side effect in patients receiving short term Prednisone medication [85]. Insomnia is defined as sleeping difficulties and occurs when body always functions during daytime. Although humankind does not have DNA photolyase but its family protein, human cryptochrome (CRY-DASH) which conserves homologous FAD region, exists in human. CRY-DASH was known as functional in regulation of body clock or circadian clock. There is no study found in the literature concerning molecular interaction of this side effect. Thus, molecular level interpretation of prednisone's short term side effect, insomnia may rely on our findings which prednisone has high binding affinity to the FAD region of DNA photolyase/cryptochrome family proteins.

Chapter 5

Conclusion

Screening a drug which targets homologous catalytic cofactor FAD region of DNA photolyase is a powerful approach to control enzymatic activity of DNA photolyase and potentially its family proteins. For this purpose, in this study, first step was virtual screening of molecular docking of 2396 FDA approved drugs (from Super Drug Database) onto the FAD region of *E. coli* DNA photolyase. *E. coli* DNA photolyase was selected to analyze photolyase/drug interaction since its three dimensional structure is obtained and the most studied enzyme among its family members. Virtual screening of molecular docking simulations were carried out and scored by AutoDock and GOLD (GoldScore Fitness), the most cited docking software.

All 2396 compounds were docked into the FAD region of photolyase, Although, FAD region was known as the active site of photolyase, it was re-validated as the binding site for small molecule drugs. Almost all drugs were bound to FAD region in their lowest binding free energy conformation. In virtual screening, some common patterns among best drug candidates were observed. In accordance with Lipinski rule of five, drugs with molecular mass smaller than 300 Da and larger than 450 Da had shown less binding affinity to FAD region. Another pattern is the presence of common substructures among best drug candidates. These sub-structures are mainly 6-membered aromatic, heterocyclic compounds (especially benzene, piperidine, piperazine, pyridine) and aryl derivatives (phenyl, phenylpropenes, phenols) and also drugs with 3-4 cyclic ring structures have higher binding affinity on photolyase.

All structural patterns are gathered as "*asymmetric polarity*". This asymmetric polarity exists in a suitable drug candidate which consists of both hydrophobic ring structures (3-4 rings) and polar structures having nitrogen and oxygen capable of forming hydrogen bonds. This proposal is also supported by the fact that residues localized on the wall of groove where FAD472 is conserved are hydrophobic on one side and polar on the other.

Furthermore, drug candidates make hydrogen bonding mostly with specific residues of the binding domain: ARG226, ASN273, GLU274, TRP277, ASN341, and FAD472. Some of these residues are crucial for the enzymatic activity. ASN273 and ASN341 were needed in creating specific binding cavity for CPD binding during DNA repair process. TRP277 serves for electron transfer mechanism during redox state of DNA repair. And FAD472 is a catalytic cofactor of the enzyme. Length of hydrogen bonds between corresponding drugs and residues vary from 1.6 Å to 2.4 Å.

Among 2396 FDA approved drugs, Eplerenone has got the lowest binding free energy (-9.06 kcal/mole, 231 nM) conformation on FAD region of DNA photolyase. Eplerenone forms 4 hydrogen bonds with 4 different residues; ARG226, ASN273, TRP277 and FAD472 with hydrogen bond length of 2.27 Å, 2.28 Å, 1.83 Å and 1.66 Å, respectively. Others high binding affinity compounds are Prednisone (K_D=316nM), Triamcinolone (K_D=982nM), Parecoxib (K_D=599nM), Azelastine (K_D=687nM) and Desloratadine (K_D=426Nm).

The last part of this study consists of experimental investigation of photolyase/drug interaction via Surface Plasmon Resonance (SPR) and compares K_D values with computational model predictions. Due to availability, only 8 of 20 shortlisted drugs, drugs were purchased as commercial drug with including inactive ingredients. Among the drugs studied, only Lornoxicam could be obtained in pure form. Drugs were dissolved in organic solvent DMSO and prepared in SPR running buffer, 1x PBS solutions with 1-100µM drug concentrations. Dilute concentrations of DMSO in PBS solution were prepared (10^{-3}-10^{-5}%). Surface immobilization of target protein was established with avidin-biotin based method. Neutravidin modified BioCap Chip was used as a sensor surface. DNA photolyase was biotinylated with Biotin-NHS conjugation. Then, immobilization of target protein was successfully established with proposed binding constants, $K_D \approx 10^{-12}$ M. Since DNA photolyase was purified as conjugated with MBP and immobilized in this form, first affinity of drugs to the MBP was also investigated in SPR. Results indicate that no specific drug binding to MBP domain exists. Nonspecific binding was minimized by adding surfactant Tween 20 into the running buffer, PBS (0.005 Tween 20). In order to remove non-specific ratio of binding from the total binding during kinetic analysis, non-specific binding to target protein was approximated in the reference channel by immobilizing another protein which has similar size and no specific binding affinity to corresponding drugs. BSA was common

protein used for this purpose, however neutravidin immobilized in BioCap Chip used in this study already satisfies these requirements as BSA. Thus possible binding of drug to immobilized neutravidin in the reference channel was considered as non-specific portion and deducted from the main channel data.

In data analysis tool, Qdat, SPR curves are fitted through the 1:1 pseudo first order kinetic model and kinetic data were calculated from these model fits. Finally, SPR results are found to be in very good agreement with computational model prediction, in terms of K_D values from both AutoDock and SPR. K_D values obtained from both pure (2.19μM) and commercial form (2.73μM) of Lornoxicam have shown close correlation with each other and computational model (8.52μM). Our assumption about neglecting the effect of inactive ingredients on binding of drugs to the FAD region of photolyase seems reasonable, as no significant effects have been observed in terms of K_D values between pure and commercial drug forms of Lornoxicam. However, this effects still needs to be further investigated for other drugs when pure forms of drug compounds could be available.

In SPR assays, Prednisone, Desloratadine, and Azelastine were found to have highest binding affinities ($K_D \approx 0.39 - 3.02$μM, $0.65 - 3.40$μM, $0.92 - 16.01$μM, respectively) to the DNA photolyase and considered as best drug candidates among drugs experimented in SPR.

Since this study focuses on FDA approved drugs, outcome of this study can reveal new side effects of these drugs or interpret existing side effects at the molecular level. In this manner, short term side effect of Prednisone should be discussed. Insomnia is the chief side effects in patients receiving short term Prednisone medication. Insomnia is defined as sleeping difficulties due to body or circadian clock abnormalities. A family protein, human cryptochrome (CRY-DASH) was known as functional in regulation of circadian clock. Thus, molecular level interpretation of prednisone's short term side effect, insomnia may rely on our findings which prednisone has high binding affinity on FAD region of DNA photolyase/cryptochrome family proteins.

The scope of this study was limited to FDA approved drugs and experimental validation of kinetic parameters of interaction between DNA photolyase and these drugs. Findings of this

study can be improved with further computational works of lead optimization with different approaches as structure modifications, molecular dynamics, etc. In addition, other family proteins like CRY-DASH can be the next target protein. Different experimental techniques such as ITC can be exploited as complementary to SPR. Finally, inhibition constants should be inevitably validated through biological inhibition assays.

APPENDIX

A1.   **Sample Docking Parameter File (DPF) - A07EA03 Prednisone on 1DNP**

```
autodock_parameter_version 4.2        # used by autodock to validate parameter set
outlev   1                            # diagnostic output level
intelec                               # calculate internal electrostatics
seed pid time                         # seeds for random generator
ligand_types C OA HD                  # atoms types in ligand
fld ..\1DNP-1.maps.fld                # grid_data_file
map ..\1DNP-1.C.map                   # atom-specific affinity map
map ..\1DNP-1.OA.map                  # atom-specific affinity map
map ..\1DNP-1.HD.map                  # atom-specific affinity map
elecmap ..\1DNP-1.e.map               # electrostatics map
desolvmap ..\1DNP-1.d.map             # desolvation map
move ..\..\..\Ligands\A07EA03.pdbqt   # small molecule
about 0.3708 0.2828 -0.4988           # small molecule center
tran0 random                          # initial coordinates/A or random
axisangle0 random                     # initial orientation
dihe0 random                          # initial dihedrals (relative) or random
tstep 2.0                             # translation step/A
qstep 50.0                            # quaternion step/deg
dstep 50.0                            # torsion step/deg
torsdof 4                             # torsional degrees of freedom
rmstol 2.0                            # cluster_tolerance/A
extnrg 1000.0                         # external grid energy
e0max 0.0 10000                       # max initial energy; max number of retries
ga_pop_size 150                       # number of individuals in population
ga_num_evals 250000                   # maximum number of energy evaluations
ga_num_generations 27000              # maximum number of generations
ga_elitism 1                          # number of top individuals to survive to next generation
ga_mutation_rate 0.02                 # rate of gene mutation
ga_crossover_rate 0.8                 # rate of crossover
ga_window_size 10.0                   #
ga_cauchy_alpha 0.0                   # Alpha parameter of Cauchy distribution
ga_cauchy_beta 1.0                    # Beta parameter Cauchy distribution
set_ga                                # set the above parameters for GA or LGA
sw_max_its 300                        # iterations of Solis & Wets local search
sw_max_succ 4                         # consecutive successes before changing rho
sw_max_fail 4                         # consecutive failures before changing rho
sw_rho 1.0                            # size of local search space to sample
sw_lb_rho 0.01                        # lower bound on rho
ls_search_freq 0.06                   # probability of performing local search on individual
set_psw1                              # set the above pseudo-Solis & Wets parameters
unbound_model bound                   # state of unbound ligand
ga_run 10                             # do this many hybrid GA-LS runs
analysis                              # perform a ranked cluster analysis
```

2. Colored Representation of Elements in Accelrys Discovery Studio 2.5

Figure A2.1 Colored Representation of Elements in Accelrys Discovery Studio 2.5

A3. Hydrogen Bonding Data from AutoDock 4.2.

*UNK0 represents the drug compound.

Hydrogen Bonding Sites	Distance (Å)	Binding Free Energy
A07EA03-		**-8.87 kcal/mole**
Prednisone		
A:ARG226:HH22 - :UNK0:O	1.84	
A:ASN341:HD22 - :UNK0:O	1.90	
:UNK0:H - A:GLU274:OE2	1.94	
A:GLY381:HN - A:ALA377:O	1.95	
A:ASN273:HD22 - :UNK0:O	2.19	
A:ARG226:HH12 - :UNK0:O	2.35	
A10BB04-		**-7.90 kcal/mole**
Glibornuride		
A:PHE150:HN - A:ASP391:OD2	2.33	
A:ARG226:HH12 - :UNK0:O	2.15	
A:FAD472:H6A1 - :UNK0:O	2.07	
:UNK0:H - A:GLU274:OE2	1.79	
:UNK0:H - A:GLU274:OE1	1.97	
B01AA01-		**-7.70 kcal/mole**
Dicoumarol		
A:ARG226:HH11 - :UNK0:O	1.94	
A:ARG226:HH11 - :UNK0:O	2.48	
A:ARG226:HH12 - :UNK0:O	2.48	
A:ASN341:HD22 - :UNK0:O	1.86	

A:FAD472:H7A - :UNK0:O   1.81

A:FAD472:H6A1 - :UNK0:O   2.48

A:FAD472:H6A2 - :UNK0:O   2.13

:UNK0:H - A:GLU274:OE1   2.11

C01BA01-   **-8.20 kcal/mole**

Quinidine

A:ASN273:HD22 - :UNK0:O   2.09

A:TRP277:HE1 - :UNK0:O   1.83

A:GLY381:HN - A:ALA377:O   1.95

A:FAD472:H6A2 - :UNK0:O   1.81

:UNK0:H - A:GLU274:OE1   1.85

C03DA04-   **-9.05 kcal/mole**

Eplerenone

A:ARG226:HH22 - :UNK0:O   2.27

A:ASN273:HD22 - :UNK0:O   2.28

A:TRP277:HE1 - :UNK0:O   1.83

A:GLY381:HN - A:ALA377:O   1.95

A:TRP384:HN - A:GLY380:O   2.34

A:FAD472:H6A1 - :UNK0:O   1.66

C10AB05-   **-6.15 kcal/mole**

Fenofibrate

A:LYS154:HZ3 - A:ASN273:OD1   2.26

A:ASN273:HD22 - :UNK0:O   2.06

A:TRP277:HE1 - :UNK0:O   2.04

G03DC04-   **-8.13 kcal/mole**

Ethisterone

A:TYR281:HH - :UNK0:O   2.18

A:ARG342:HH22 - :UNK0:O   2.08

:UNK0:H - A:TYR281:OH   2.19

G03GB02-   **-5.95 kcal/mole**

Clomifene

A:PHE150:HN - A:ASP391:OD2   2.33

A:ARG342:HH21 - A:ASP227:OD1   2.37

M01AC05-   **-6.92 kcal/mole**

Lornoxicam

:UNK0:H - A:GLU274:OE1   2.19

:UNK0:HN - A:GLU274:OE2   2.13

A:ARG342:HH21 - A:ASP227:OD1   2.37

A:ASN273:HD22 - :UNK0:O   1.93

A:TRP277:HE1 - :UNK0:O   1.83

A:TRP384:HE1 - :UNK0:O   2.29

A:TYR222:HH - A:FAD472:O2A   1.89

M01AH02-   **-7.93 kcal/mole**

Rofecoxib

A:PHE150:HN - A:ASP391:OD2   2.33

A:ARG226:HH11 - :UNK0:O   1.75

A:ASN341:HD21 - :UNK0:O   1.98

A:ALA385:HN - A:GLY381:O   2.19

M01AH04-   **-8.49 kcal/mole**

Parecoxib

A:TYR222:HH - A:FAD472:O2A   1.89

A:ARG226:HH11 - :UNK0:O   1.80

A:ASN341:HD21 - :UNK0:O   2.11

A:FAD472:H1 - A:FAD472:O3'   2.18

A:FAD472:H2' - A:FAD472:O4'   1.68

M09AA01-   **-7.53 kcal/mole**

Hydroquinine

A:ASN273:HD22 - :UNK0:O   2.06

A:TRP277:HE1 - :UNK0:O   1.94

A:ARG342:HH21 - A:ASP227:OD1 2.37

A:FAD472:H6A2 - :UNK0:O   2.26

:UNK0:H - A:GLU274:OE1   2.38

N05AF04-   **-8.14 kcal/mole**

Tiotixene

A:TYR222:HH - A:FAD472:O2A   1.89

A:TYR281:HH - :UNK0:O   2.05

A:FAD472:H6A1 - :UNK0:O   2.05

A:FAD472:H6A1 - :UNK0:O   2.27

A:FAD472:H6A2 - :UNK0:O   2.33

N07BB04-   **-7.86 kcal/mole**

Naltrexone

A:TYR281:HH - :UNK0:O   2.33

A:TYR281:HH - :UNK0:O   2.07

A:ASN341:HD22 - :UNK0:O   2.46

A:ARG342:HH21 - A:ASP227:OD1 2.37

A:TRP384:HN - A:GLY380:O   2.34

A:FAD472:H6A2 - :UNK0:O   2.35

:UNK0:H - A:ASN341:OD1   2.14

:UNK0:H - A:ASP391:O   2.32

N07CA02-   **-7.92 kcal/mole**

Cinnarizine

A:TYR222:HH - A:FAD472:O2A   1.89

P03BA02-   **-5.46 kcal/mole**

Cypermethrin

A:ASN341:HD22 - :UNK0:O   1.90

A:ARG342:HH21 - A:ASP227:OD1 2.37

R06AE05-   **-8.17 kcal/mole**

Meclozine

A:ASN341:HD22 - :UNK0:N   2.36

R06AX19-   **-8.41 kcal/mole**

Azelastine

A:ASN341:HD21 - :UNK0:O   2.48

A:ARG342:HH21 - A:ASP227:OD1 2.37

A:TRP384:HN - A:GLY380:O   2.34

A:ALA385:HN - A:GLY381:O   2.19

:UNK0:HN - A:GLU274:OE1   2.29

R06AX27-   **-8.76 kcal/mole**

Desloratadine

A:PHE150:HN - A:ASP391:OD2   2.33

A:ALA385:HN - A:GLY381:O   2.19

:UNK0:H - A:GLU274:OE1   2.23

:UNK0:H - A:GLU274:OE2   1.69

R06AX28-   **-8.14 kcal/mole**

Rupatadine

A:PHE150:HN - A:ASP391:OD2   2.33

A:TYR222:HH - A:FAD472:O2A   1.89

A4.   Determination of DNA Photolyase Concentration

Table A3.1 Standard Curve Data of BSA

STANDARD CURVE					
Volume of BSA added [ul]	Final Volume [ul]	Concentration (BSA) [mg/ml]	Concentration (BSA) [mg/ml]	Concentration (BSA) [ug/ml]	Absorbance at (595 nm)
0	1000	0	0	0	0
2	1002	0.00199	0.002	1.99	0.056
4	1004	0.00398	0.004	3.98	0.139
6	1006	0.00596	0.006	5.96	0.283
8	1008	0.00793	0.008	7.93	0.295
10	1010	0.00990	0.010	9.90	0.330

Table A3.2 Protein Sample Data

Photolyase Sample					
Sample fraction	Absorbance at (595 nm)	Concentration (sample in eppendorf) [ug/ml]	Volume (sample) [ml]	Concentration (main sample) [ug/ml]	Mass (sample) [mg]
1-3	0.537	14.91	1	1506.58	1.50
1-4	0.227	6.30	1	636.81	0.63
2-3	0.298	8.27	1	836.05	0.83
3-8	0.186	5.16	1.5	521.83	0.78
3-9	0.306	8.50	1.5	858.50	1.28
3-10	0.069	1.91	1.5	193.58	0.29
4-7	0.075	2.08	1.5	210.41	0.31
4-8	0.250	6.94	1.5	701.38	1.05
4-9	0.188	5.22	1.5	527.44	0.79
4-10	0.054	1.50	1.5	151.50	0.22
					Total = 7.72

A5. Technical Specifications a SensiQ Discovery (ICX Nomadics, USA)

*Following data taken from ICX Nomadics Technologies Product Overview, sensiq@icxt.com

Specifications

Real time reference curve subtraction	Yes
Flow cell volume	50nl
Simultaneous injection	Yes
Injection volume	10 to 250 µl
Refractive index range	1.33 – 1.40
Short time noise	< 1 RU
Flow rate	User configurable
Sample injector	Manual actuation
Sample loops	2 (independently loaded)
Temperature	Room temperature

Working Ranges

k_a	$1 \times 10^8 \, M^{-1} \, s^{-1}$
k_d	$10^{-1} – 10^{-6} \, s^{-1}$
Concentration	$10^{-3} – 10^{-11} \, M$

A6.   Drug Information

*All following information was taken from http://drugbank.ca [44].

Drug Name: Lornoxicam (ATC Code – M01AC05)

Brand: Xeforapid

Formula: $C_{13}H_{10}ClN_3O_4S_2$

Molecular Weight: 371.81 g/mol
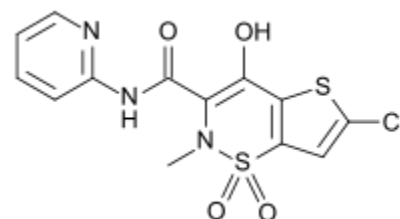
Description: Lornoxicam is a new nonsteroidal drug and it is used as anti-inflammatory drug (NSAID). Its family is from oxicam and as well good as an analgesic and antipyretic. However, Lornoxicam differs from the oxicam family with its potential of inhibiting the prostaglandin biosynthesis and its particular efficacy is explained with this difference.

Side Effects: Lornoxicam does not have any unique side effect when compared to the other anti-inflammatory drugs. Common side effects are related with gastrointestinal disorder, such as nausea and diarrhea, and headache. Rarely, bleeding and bronchospasms can occur and Stevens-Johnson syndrome may occur extremely rare. However, those seldom side effects can be severe.

Properties:

water solubility	4.61e-02 g/l
logP	2.53
logP	1.85
Logs	-3.91
pKa	13.63
hydrogen acceptor count	6
hydrogen donor count	2
polar surface area	99.60
rotatable bond count	2
Refractivity	97.02
polarizability	33.77

Drug Name: Prednisone (ATC Code –A07EA03 H02AB07)

Brand: Deltacortil

Formula: $C_{21}H_{26}O_5$

Molecular Weight: 358.42 g/mol
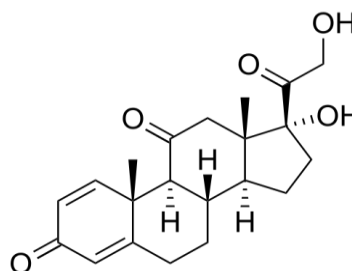
Description: Prednisone is a synthetic anti-inflammatory drug and it is a derivative of corticosteroids. Its main effectiveness occurs as an immunosuppressant. Other than inflammatory treatment, it is also used in treatment of cancer. Although it is synthetic, this drug is biologically inert and it can be converted to prednisolone in the liver.

Side Effects: Since Prednisone suppresses the immune system, it could make the person more delicate and fragile to infections. Short term side effects do not differ much from the regular glucocorticoids and it results in high blood glucose level. Other than that, insomnia, euphoria and bipolar disorder are observed with the short term usage. Cushing's syndrome, truncal weight gain, osteoporosis, glaucoma and cataracts can be counted in long term side effects.

Properties:

water solubility	1.11e-01 g/l
logP	2.07
logP	1.66
Logs	-3.51
pKa	13.90
hydrogen acceptor count	5
hydrogen donor count	2
polar surface area	91.67
rotatable bond count	2
Refractivity	97.57
polarizability	38.17

Drug Name: Azelastine (ATC Code – R06AX19)

Brand: Allergodil Nazal Sprey

Formula: $C_{22}H_{24}ClN_3O$
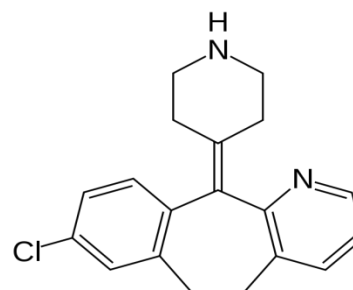
Molecular Weight: 381.89 g/mol
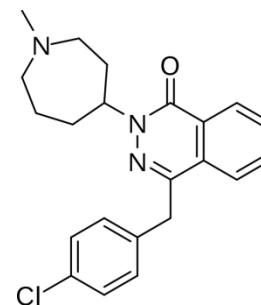
Description: Azelastine is a second generation antihistamine which is a derivative of phthalazine. Just manipulating the volume ratio, azelastine can be used both as a nasal spray and as an eye drop.

Side Effects: Azelastine is very safe for the body and it is well tolerated by the children as well. Reported side effects are bitter taste, headache, nasal burning and somnolence.

Properties:

water solubility	9.20e-03 g/l
logP	3.81
logP	4.04
Logs	-4.62
pKa	-
hydrogen acceptor count	3
hydrogen donor count	0
polar surface area	35.91
rotatable bond count	3
Refractivity	110.52
Polarizability	41.54

Drug Name: Desloratadine (ATC Code –R06AX27)

Brand: Deloday

Formula: $C_{19}H_{19}ClN_2$

Molecular Weight: 310.82 g/mol

Description: Desloratadine is used for treating allergies and it is a tricyclic antihistamine. It is second generation histamine, in other words it is the active descarboethoxy metabolite of loratidine. Its effect lasts long and it does not cause drowsiness because it takes some time to go into the central nervous system.

Side Effects: Fatigue, dry mouth, headache and gastrointestinal disturbances are most commonly observed side effects.

Properties:

water solubility	3.95e-03 g/l
logP	3.48
logP	3.97
Logs	-4.90
pKa	-
hydrogen acceptor count	2
hydrogen donor count	1
polar surface area	24.92
rotatable bond count	0
Refractivity	101.04
Polarizability	34.35

Drug Name: Rupatadine (ATC Code –R06AX28)

Brand: Rupafin
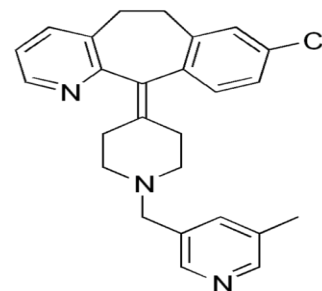
Formula:C$_{26}$H$_{26}$ClN$_3$
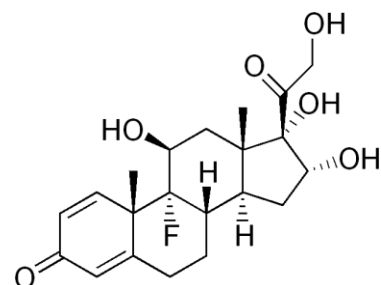
Molecular Weight: 415.95 g/mol

Description: Rupatadine is a second generation antihistamine and PAF antagonist which is used to treat allergies.

Side Effects: Rupatadine does not have any strong side effect; however, as in the case of other antihistamines, it can cause somnolence, headaches and fatigue.

Drug Name: Triamcinolone (ATC Code –R03BA06)

Brand: Sinakort A

Formula: $C_{21}H_{27}FO_6$

Molecular Weight: 394.43 g/mol

Description: Triamcinolone is a synthetic corticosteroid and its effect lasts long. Since it is free of alcohol or esterified forms, it can be taken orally, intramuscularly, by injection or as a topical ointment.

Side Effects: Sore throat, nose bleeding, coughing, headache or runny noses are common side effects of Triamcinolone. If white patches occur in the throat or nose, care should be taken. Women may suffer additional side effect by having a prolonged menstrual cycle.

Properties:

water solubility	8.47e-01 g/l
logP	0.84
logP	0.24
Logs	-2.67
pKa	13.40
hydrogen acceptor count	6
hydrogen donor count	4
polar surface area	115.06
rotatable bond count	2
Refractivity	99.38
polarizability	39.79

Drug Name: Fenofibrate (ATC Code –C10AB05)

Brand: Lipanthy 267
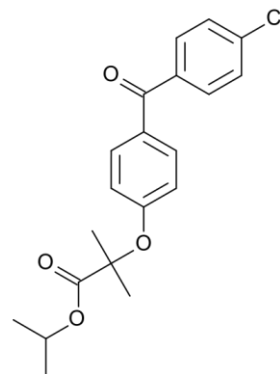
Formula: $C_{20}H_{21}ClO_4$

Molecular Weight: 360.83 g/mol

Description: Fenofibrate is a drug used to reduce the cholesterol levels in patients at risk of cardiovascular disease. It's from the fibrate class and like other fibrates it reduces both low density lipoprotein (LDL) and very low density lipoprotein (VLDL) levels. On the other hand, it increases high density lipoprotein metabolic syndrome.

Side Effects: Gastrointestinal problems such as digestive, gastric, intestinal disorders, abdominal pain, nausea, vomiting, diarrhea, flatulence. However, more importantly it causes skin reactions, rashes, pruritus, urticaria or photosensitivity reactions.

Drug Name: Clomifene (ATC Code –G03GB02)

Brand: Serophene 50
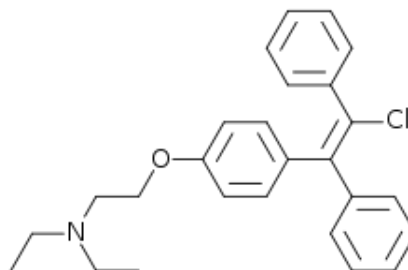
Formula: $C_{26}H_{28}ClNO$

Molecular Weight: 405.96 g/mol

Description: Clomifene is also called as clomiphene is a triphenyl ethylene stillbene derivative. In other words, it is a selective estrogen receptor modulator. It increases the production of gonadotropins by inhibiting the negative feedback on the hypothalamus. It is used for the treatment of female infertility.

Side Effects: A very common adverse effect is the hot flashes, abdominal discomfort, visual blurring and reversible ovarian enlargement or cyst formation. 1% of patients reported abnormal uterine bleeding, nausea or vomiting. Rare adverse effects which are less than 0.1% of patience reported reversible alopecia or ovarian hyperstimulation syndrome.

Properties:

water solubility	4.14e-04 g/l
logP	6.08
logP	6.47
Logs	-5.99
pKa	-
hydrogen acceptor count	2
hydrogen donor count	0
polar surface area	12.47
rotatable bond count	9
Refractivity	133.76
polarizability	46.74

Bibliography

[1] Drews, J., *Drug discovery: a historical perspective.* Science, 2000. **287**(5460): p. 1960-4.

[2] Madsen, U.K.-L., Povl; Liljefors, Tommy, *Textbook of Drug Design and Discovery*. 2002, Washington, DC: Taylor & Francis.

[3] Drews, J., *Case histories, magic bullets and the state of drug discovery.* Nat Rev Drug Discov, 2006. **5**(8): p. 635-40.

[4] Overington, J.P., B. Al-Lazikani, and A.L. Hopkins, *Opinion - How many drug targets are there?* Nature Reviews Drug Discovery, 2006. **5**(12): p. 993-996.

[5] Sancar, A., *Structure and function of DNA photolyase and cryptochrome blue-light photoreceptors.* Chem Rev, 2003. **103**(6): p. 2203-37.

[6] Guo, H., et al., *The Arabidopsis blue light receptor cryptochrome 2 is a nuclearprotein regulated by a blue light-dependent post-transcriptional mechanism.* The Plant Journal, 1999. **19**(3): p. 279-287.

[7] Lengauer, T. and M. Rarey, *Computational methods for biomolecular docking.* Curr Opin Struct Biol, 1996. **6**(3): p. 402-6.

[8] Morris, G.M., et al., *Automated docking using a Lamarckian genetic algorithm and an empirical binding free energy function.* Journal of Computational Chemistry, 1998. **19**(14): p. 1639-1662.

[9] Huey, R., et al., *A semiempirical free energy force field with charge-based desolvation.* Journal of Computational Chemistry, 2007. **28**(6): p. 1145-1152.
[10] Verdonk, M.L., et al., *Improved protein-ligand docking using GOLD.* Proteins, 2003. **52**(4): p. 609-23.

[11] Morris, G.M., et al., *AutoDock4 and AutoDockTools4: Automated docking with selective receptor flexibility.* J Comput Chem, 2009. **30**(16): p. 2785-91.

[12] Morris, G.M., et al., *Distributed automated docking of flexible ligands to proteins: parallel applications of AutoDock 2.4.* J Comput Aided Mol Des, 1996. **10**(4): p. 293-304.

[13] Huey, R., et al., *Grid-Based Hydrogen Bond Potentials with Improved Directionality.* Letters in Drug Design & Discovery, 2004. **1**(2): p. 178-183.

[14] Goodsell, D.S. and A.J. Olson, *Automated Docking of Substrates to Proteins by Simulated Annealing.* Proteins-Structure Function and Genetics, 1990. **8**(3): p. 195-202.

[15] Sancar, A. and C.S. Rupert, *Cloning of the phr gene and amplification of photolyase in Escherichia coli.* Gene, 1978. **4**(4): p. 295-308.

[16] Sancar, A., *Structure and function of DNA photolyase.* Biochemistry, 1994. **33**(1): p.2-9.

[17] Gasteiger, J. and M. Marsili, *Iterative partial equalization of orbital electronegativity—a rapid access to atomic charges.* Tetrahedron, 1980. **36**(22): p. 3219-3228.

[18] http://autodock.scripps.edu/, last visited 15.08.2011.

[19] Wolf, L.K., *digital briefs.* Chemical & Engineering News, 2009. **87**(5): p. 32.

[20] http://www.ccdc.cam.ac.uk/support/documentation/gold/5_0/gold/, last visited 15.08.2011.

[21] Verdonk, M.L., et al., *Improved protein-ligand docking using GOLD.* Proteins, 2003.**52**(4): p. 609-23.

[22] Eldridge, M.D., et al., *Empirical scoring functions: I. The development of a fast empirical scoring function to estimate the binding affinity of ligands in receptor complexes.* Journal of Computer-Aided Molecular Design, 1997. **11**(5): p. 425-445.

[23] Selby, C.P. and A. Sancar, *Molecular mechanisms of DNA repair inhibition by caffeine.* Proc Natl Acad Sci U S A, 1990. **87**(9): p. 3522-5.

[24] Buchholz, G., B. Ehmann, and E. Wellmann, *Ultraviolet Light Inhibition of Phytochrome-Induced Flavonoid Biosynthesis and DNA Photolyase Formation in Mustard Cotyledons (Sinapis alba L.).* Plant Physiology, 1995. **108**(1): p. 227-234.

[25] Zhao, S. and A. Sancar, *Human Blue-light Photoreceptor hCRY2 Specifically Interacts with Protein Serine/Threonine Phosphatase 5 and Modulates Its Activity.* Photochemistry and Photobiology, 1997. **66**(5): p. 727-731.

[26] Jarillo, J.A., et al., *An Arabidopsis circadian clock component interacts with both CRY1 and phyB.* Nature, 2001. **410**(6827): p. 487-490.

[27] Park, H., et al., *Crystal structure of DNA photolyase from Escherichia coli.* Science, 1995. **268**(5219): p. 1866-1872.

[28] Malhotra, K., et al., *Putative Blue-Light Photoreceptors from Arabidopsis thaliana and Sinapis alba with a High Degree of Sequence Homology to DNA Photolyase Contain the Two Photolyase Cofactors but Lack DNA Repair Activity.* Biochemistry, 1995. **34**(20): p. 6892-6899.

[29] Bernstein, F.C., et al., *The protein data bank: A computer-based archival file for macromolecular structures.* Journal of Molecular Biology, 1977. **112**(3): p. 535-542.

[30] Gwendolyn B, S., *DNA photolyases: Physical properties, action mechanism, and roles in dark repair.* Mutation Research/DNA Repair. **236**(2-3): p. 147-160.

[31] Li, Y.F. and A. Sancar, *Active site of Escherichia coli DNA photolyase: mutations at Trp277 alter the selectivity of the enzyme without affecting the quantum yield of photorepair.* Biochemistry, 1990. **29**(24): p. 5698-5706.

[32] Lipinski, C.A., et al., *Experimental and computational approaches to estimate solubility and permeability in drug discovery and development settings.* Advanced Drug Delivery Reviews, 2001. **46**(1-3): p. 3-26.

[33] Emsley, J., *Very strong hydrogen bonding.* Chemical Society Reviews, 1980. **9**(1): p. 91-124.

[34] Sancar, A., et al., *Purification and characterization of three members of the photolyase/cryptochrome family blue-light photoreceptors from Vibrio cholerae.* Journal of Biological Chemistry, 2003. **278**(40): p. 39143-39154.

[35] Sambrook, J., Fritsch, E.F. & Maniatis, T. *Molecular Cloning: A Laboratory Manual* 2nd edn Cold Spring Harbor Laboratory Press, 1989. **25**(1): p. 1-15.

[36] Sambrook, J., Fritsch, E.F. & Maniatis, T. *Molecular Cloning: A Laboratory Manual* 3nd edn Cold Spring Harbor Laboratory Press, 1991. **44**(4): p. 13-14.

[37] Bloch, K.D., et al., *cDNA cloning and chromosomal assignment of the gene encoding endothelin 3.* Journal of Biological Chemistry, 1989. **264**(30): p. 18156-61.

[38] Maniatis, T, Sambrook, J., Fritsch, E.F. *Molecular Cloning: A Laboratory Manual* 1nd edn Cold Spring Harbor Laboratory Press, 1980. **11**(1): p. 4-9.

[39] Sasse J., *Current Protocols in Molecular Biology* 1989. **10**(6): p. 1-10.

[40] F.M.Ausebel et al., *Current Protocols in Molecular Biology* 1989. **10**(8): p. 11-21.

[41] Hertzberg, R.P. and A.J. Pope, *High-throughput screening: new technology for the 21st century.* Current Opinion in Chemical Biology, 2000. **4**(4): p. 445-451.

[42] Hann, M.M. and T.I. Oprea, *Pursuing the leadlikeness concept in pharmaceutical research.* Current Opinion in Chemical Biology, 2004. **8**(3): p. 255-263.

[43] Chapman, T., *Drug discovery: The leading edge.* Nature, 2004. **430**(6995): p. 109-115.

[44] Swinney, D.C., *Biochemical mechanisms of drug action: what does it take for success?* Nat Rev Drug Discov, 2004. **3**(9): p. 801-8.

[45] Myszka, D.G. and R.L. Rich, *Implementing surface plasmon resonance biosensors in drug discovery.* Pharmaceutical Science & Technology Today, 2000. **3**(9): p.310-317.

[46] Liedberg, B., C. Nylander, and I. Lundstrom, *Surface-Plasmon Resonance for Gas-Detection and Biosensing.* Sensors and Actuators, 1983. **4**(2): p. 299-304.

[47] Cunningham, B.C. and J.A. Wells, *Comparison of a Structural and a Functional Epitope.* Journal of Molecular Biology, 1993. **234**(3): p. 554-563.

[48] Johanson, K., et al., *Binding Interactions of Human Interleukin-5 with Its Receptor-Alpha Subunit - Large-Scale Production, Structural, and Functional, Studies of Drosophila-Expressed Recombinant Proteins.* Journal of Biological Chemistry, 1995. **270**(16): p. 9459-9471.

[49] Holliger, P., T. Prospero, and G. Winter, *Diabodies - Small Bivalent and Bispecific Antibody Fragments.* Proceedings of the National Academy of Sciences of the United States of America, 993. **90**(14): p. 6444-6448.

[50] Kelley, R.F. and M.P. Oconnell, *Thermodynamic Analysis of an Antibody Functional Epitope.* Biochemistry, 1993. **32**(27): p. 6828-6835.

[51] Malmborg, A.C. and C.A.K. Borrebaeck, *Biacore as a Tool in Antibody Engineering.* Journal of Immunological Methods, 1995. **183**(1): p. 7-13.

[52] Glaser, M., et al., *Myristoylated alanine-rich C kinase substrate (MARCKS) produces reversible inhibition of phospholipase C by sequestering phosphatidylinositol 4,5-bisphosphate in lateral domains.* Journal of Biological Chemistry, 1996. **271**(42): p. 26187-26193.

[53] Madrigal, L., et al., *Flow Cytometric Analysis of Surface Major Histocompatibility Complex Class-Ii Expression on Human Epithelial-Cells Prepared from Small Intestinal Biopsies.* Journal of Immunological Methods, 1993. **158**(2): p. 207-214.

[54] Strasser D., *Real Time Drug Discovery,* University of Basel, Faculty of Science, 2008

[55] Ricklin D., *Surface Plasmon Resonance Applications in Drug Discovery*, University of Basel, Faculty of Science, 2005.

[56] Surface Plasmon Resonance (Technology Note 1*), Biacore AB* 2001.

[57] Jonsson, U., et al., *Real-Time Biospecific Interaction Analysis Using Surface- Plasmon Resonance and a Sensor Chip Technology.* Biotechniques, 1991. **11**(5): p. 620-&.

[58] Nagata, K.,Handa, H*., Real-Time Analysis of Biomolecular Interactions: Applications of Biacore,* Springer, 2000.

[59] Schasfoort, R.B.M. and A.J. Tudos, *Handbook of surface plasmon resonance,* Cambridge, UK: RSC Pub., 2008. **21**: p. 403.

[60] Fisher, R.J. and M. Fivash, *Surface plasmon resonance based methods for measuring the kinetics and binding affinities of biomolecular interactions.* Current Opinion in Biotechnology, 1994. **5**(4): p. 389-395.

[61] Di Primo, C. and I. Lebars, *Determination of refractive index increment ratios for protein–nucleic acid complexes by surface plasmon resonance.* Analytical Biochemistry, 2007. **368**(2): p. 148-155.

[62] Demir E., *Characterization of Real Time DNA Repair via Surface Plasmon Resonance (SPR),* Koc University, Institute of Science and Engineering, 2011.

[63] Johnsson, B., et al., *Comparison of methods for immobilization to carboxymethyl dextran sensor surfaces by analysis of the specific activity of monoclonal antibodies.* Journal of Molecular Recognition,1995. **8**(1-2): p. 125-131.

[64] Stein, T. and G. Gerisch, *Oriented Binding of a Lipid-Anchored Cell Adhesion Protein onto a Biosensor Surface Using Hydrophobic Immobilization and Photoactive Crosslinking.* Analytical Biochemistry,1996. **237**(2): p. 252-259.

[65] Bernard, A. and H.R. Bosshard, *Real-Time Monitoring of Antigen-antibody, Recognition on a Metal Oxide Surface by an Optical Grating Coupler Sensor.* European Journal of Biochemistry, 1995. **230**(2): p. 416-423.

[66] Roos, H., et al., *Thermodynamic analysis of protein interactions with biosensor technology.* Journal of Molecular Recognition, 1998. **11**(1-6): p. 204-210.

[67] Bio-Rad Laboratories Inc, *Protein interaction analysis bulletin,* 2011. **6044:** Rev.

[68] Stefan, W., *Light-driven enzymatic catalysis of DNA repair: a review of recent biophysical studies on photolyase.* Biochimica et Biophysica Acta (BBA) - Bioenergetics, 2005. **1707**(1): p. 1-23.

[69] Daniel J, O.S., *Determination of kinetic rate and equilibrium binding constants for macromolecular interactions: a critique of the surface plasmon resonance literature.* Current Opinion in Biotechnology, 1994. **5**(1): p. 65-71.

[70] van der Merwe, P.A., *Surface Plasmon Resonace*, Oxford University Press, 2001. **185**(3): p. 137-170.

[71] Lu, M., et al., *XIAP Induces NF-κB Activation via the BIR1/TAB1 Interaction and BIR1 Dimerization.* Molecular Cell, 2007. **26**(5): p. 689-702.

[72] BIACORE AB, *Bia Journal*,1998. **2**: p. 18.

[73] Schuck, P. and A.P. Minton, *Analysis of Mass Transport-Limited Binding Kinetics in Evanescent Wave Biosensors.* Analytical Biochemistry, 1996. **240**(2): p. 262-272.

[74] Northrup, S.H. and H.P. Erickson, *Kinetics of protein-protein association explained by Brownian dynamics computer simulation.* Proceedings of the National Academy of Sciences, 1992. **89**(8): p. 3338-3342.

[75] Schwartz, M., et al., *Further Studies on the Binding of Maltose to the Maltose- Binding Protein of Escherichia coli.* European Journal of Biochemistry, 1976. **71**(1): p.167-170.

[76] Felder, S., et al., *Sh2 Domains Exhibit High-Affinity Binding to Tyrosine- Phosphorylated Peptides yet Also Exhibit Rapid Dissociation and Exchange.* Molecular and Cellular Biology, 1993. **13**(3): p. 1449-1455.

[77] Davis, S.J. and P.A. van der Merwe, *The structure and ligand interactions of CD2: implications for T-cell function.* Immunology Today, 1996. **17**(4): p. 177-187.

[78] Glaser, R.W., *Antigen-Antibody Binding and Mass-Transport by Convection and Diffusion to a Surface - a 2-Dimensional Computer-Model of Binding and Dissociation Kinetics.* Analytical Biochemistry, 1993. **213**(1): p. 152-161.

[79] Chen, L., et al., *Discovering Severe Acute Respiratory Syndrome Coronavirus 3CL Protease Inhibitors: Virtual Screening, Surface Plasmon Resonance, and Fluorescence Resonance Energy Transfer Assays.* Journal of Biomolecular Screening, 2006. **11**(8): p. 915-921.

[80] Lu, I.L., et al., *Structure-Based Drug Design and Structural Biology Study of Novel Nonpeptide Inhibitors of Severe Acute Respiratory Syndrome Coronavirus Main Protease.* Journal of Medicinal Chemistry, 2006. **49**(17): p. 5154-5161.

[81] Du, L., et al., *Binding Investigation of Human 5-Lipoxygenase with Its Inhibitors by SPR Technology Correlating with Molecular Docking Simulation.* Journal of Biochemistry, 2006. **139**(4): p. 715-723.

[82] Nomadics Inc., *Qdat Tutorial,* 2007.

[83] Angerer, L., et al., *An electron microscope study of the relative positions of the 4S and ribosomal RNA genes in HeLa cell mitochondrial DNA.* Cell, 1976. **9**(1): p. 81-90.

[84] http://drugbank.ca/drugs/, last visited 25.08.2011.

[85] Lozada, F., S. Silverman, and C. Migliorati, *Adverse side effects associated with prednisone in the treatment of patients with oral inflammatory ulcerative diseases.* The Journal of the American Dental Association, 1984. **109**(2): p. 269-270.

VITA

Selimcan Azizoğlu was born in Diyarbakır, 1985. He graduated from Diyarbakır Fen Lisesi in 2003 as the most successful student among other graduates. Same year, he started his study in Chemical & Biological Engineering at Koç University, İstanbul. In 2008, he received his B.S. degree. In 2009, he came back to Koç University to study M.S. in Chemical and Biological Engineering.